



# Polydopamine-cladded montmorillonite micro-sheets as therapeutic platform repair the gut mucosal barrier of murine colitis through inhibiting oxidative stress



Gaolong Lin<sup>a</sup>, Fengnan Yu<sup>a</sup>, Dingwei Li<sup>a</sup>, Yi Chen<sup>a</sup>, Mengjiao Zhang<sup>a</sup>, Kaili Lu<sup>b</sup>, Neili Wang<sup>a</sup>, Sunkuan Hu<sup>c</sup>, Yingzheng Zhao<sup>a,\*\*</sup>, Helin Xu<sup>a,\*</sup>

<sup>a</sup> Department of Pharmaceutics, School of Pharmaceutical Sciences, Wenzhou Medical University, Wenzhou City, Zhejiang Province, 325035, China

<sup>b</sup> Cixi Biomedical Research Institute of Wenzhou Medical University, China

<sup>c</sup> Department of Gastroenterology, The First Affiliated Hospital of Wenzhou Medical University, Wenzhou City, Zhejiang Province, 325000, China

## ARTICLE INFO

### Keywords:

Montmorillonite  
Polydopamine  
Ulcerative colitis  
Oxidative stress  
Gut mucosal barrier

## ABSTRACT

Montmorillonite (MMT), a layered aluminosilicate, has a mucosal nutrient effect and restores the gut barriers integrity. However, orally administrating MMT is not effective to combat the reactive oxygen species (ROS) and alleviate the acute inflammatory relapse for colitis patients. Herein, polydopamine-doped montmorillonite micro-sheets (PDA/MMT) have been developed as a therapeutic platform for colitis treatment. SEM and EDS analysis showed that dopamine monomer (DA) was easily polymerized in alkaline condition and polydopamine (PDA) was uniformly cladded on the surface of MMT micro-sheets. The depositing amount of PDA was reaching to  $2.06 \pm 0.08\%$ . Moreover, *in vitro* fluorescence probes experiments showed that PDA/MMT presented the broad spectra of scavenging various ROS sources including  $\bullet\text{OH}$ ,  $\bullet\text{O}_2^-$ , and  $\text{H}_2\text{O}_2$ . Meanwhile, the intracellular ROS of Rospup/ $\text{H}_2\text{O}_2$  treated Caco-2 cell was also effectively scavenged by PDA/MMT, which resulted in the obvious improvement of the cell viability under oxidative stress. Moreover, most of orally administrated PDA/MMT was transited to the gut and form a protective film on the diseased colon. PDA/MMT exhibited the obvious therapeutic effect on DSS-induced ulcerative colitis mouse. Importantly, the gut mucosa of colitis mouse was well restored after PDA/MMT treatment. Moreover, the colonic inflammation was significantly alleviated and the goblet cells were obviously recovered. The therapeutic mechanism of PDA/MMT was highly associated with inhibiting oxidative stress. Collectively, PDA/MMT micro-sheets as a therapeutic platform may provide a promising therapeutic strategy for UC treatment.

## 1. Introduction

Ulcerative colitis (UC) is a chronic inflammatory bowel disease affecting the colon and rectum with chronic and idiopathic inflammation [1]. UC is characterized by the continuous but more superficially inflamed mucosa. The pathogenesis of UC is commonly relevant to the dysregulation of systemic immune, the mucosal inflammation, and the impairment of the epithelial barrier integrity [2–4]. UC is imposing increasing health and economic burden worldwide, with the highest prevalence in developed countries. Despite the low deaths over world, UC still adversely affects the quality of an individual's life [5,6]. The common UC regimens are using mesalazine/5-ASA, corticosteroids, or

immunosuppressants (cyclosporine or tacrolimus) to alleviate the flaring inflammatory response and maintain the remission in terms of its severity into the mild, moderate, or severe category. The next escalation therapy is intravenous or subcutaneous TNF- $\alpha$  immunotherapy (infliximab; adalimumab, golimumab) [7]. However, due to the severe side effect of traditional therapeutics and the high population of nonresponders or loss-of-response in case of biologic immunotherapy, a certain population of patients remain without satisfying treatment options [8]. Moreover, all these treatment strategies make patients confront the increased risk of infection. Hence, further expansion of the therapeutic horizons is highly desirable for the management of UC.

Previous studies have found that reactive oxygen species (ROS)

\* Corresponding author.

\*\* Corresponding author.

E-mail addresses: [pharmtds@163.com](mailto:pharmtds@163.com) (Y. Zhao), [xhlpharm1214@126.com](mailto:xhlpharm1214@126.com) (H. Xu).

<https://doi.org/10.1016/j.mtbio.2023.100654>

Received 30 March 2023; Received in revised form 28 April 2023; Accepted 1 May 2023

Available online 3 May 2023

2590-0064/© 2023 The Authors. Published by Elsevier Ltd. This is an open access article under the CC BY-NC-ND license (<http://creativecommons.org/licenses/by-nc-nd/4.0/>).

overproduction and thus oxidative stress played important roles in the initiation and progression of UC [9,10]. It has now been reported that the inflamed colons of UC patients present 10- to 100-fold higher ROS level than that of the unaffected colon [11,12]. Under the pathological conditions of UC, the neutrophils are activated and recruited to the inflamed colon, where ROS sources, for example, hydrogen peroxide ( $H_2O_2$ ), hydroxyl radicals ( $\cdot OH$ ), and superoxide anion ( $O_2^{\cdot -}$ ) were produced. Excessive ROS disrupts redox homeostasis and further triggers oxidative damage to epithelium and related proteins or DNA, destroying the integrity of the gut mucosal barrier [13]. Restoration of the gut mucosal barrier is considered to be a promising approach in the management of colitis. Intestinal mucosal healing, epithelial restitution, and symptom management have become essential to sustain the remission of UC. Some natural anti-oxidative molecules, inorganic nanoenzyme, or natural enzymes have been developed to scavenge ROS for ulcerative colitis treatment [14,15]. However, the removal activity against just a kind of ROS was generally achieved for these natural small molecules or enzymes [16]. Usage of inorganic nanoenzyme is potentially toxic in the long term and not environmentally friendly [17–19]. Moreover, the mucosal healing of the inflamed colon was not well achieved for these regimens.

Montmorillonite (MMT), an inorganic clay mineral layered aluminosilicate, has been approved as an antidiarrheal agent for over 40 years [20]. MMT displays 2:1-layered TOT sheets consisting of one Al–O octahedral (O) sheet sandwiched by two Si–O tetrahedral (T) sheets. Due to the partially isomorphous substitution of  $Si^{4+}$  by  $Al^{3+}$  in the silica tetrahedral sheets and  $Al^{3+}$  by  $Mg^{2+}$  in the alumina octahedral sheets, MMT has the net negative charge and usually adsorbs the exchangeable cations such as  $Li^+$ ,  $Na^+$ , and  $Ca^{2+}$  inside the layers. Due to its high cation exchange capacity, MMT undergoes ion exchange with basic drugs or cations in solution within their interlayer space. Moreover, these layered MMT clay can be fine-exfoliated to yield micro/nano-sheets with a high aspect ratio [21]. Orally administrating such exfoliated MMT can interact with the mucus glycoproteins and thus form a physical barrier on the intestinal mucosa without systematic absorption or interfering with normal colonic function [22,23]. Moreover, the exfoliated MMT micro-sheets present gastro-protective activity against the inflamed microenvironment due to its neutralizing gastric acidity. Besides, recent studies suggest that MMT also has a mucosal nutrient effect and thus restores the integrity of intestinal epithelial cells and barriers, accommodating its application in the treatment of UC [24]. However, there exists the risk of constipation for some UC

patients post orally administrating MMT due to its insufficient ROS elimination and anti-inflammatory ability.

Polydopamine (PDA) as a natural biopolymer is facilely prepared by the oxidative polymerization of dopamine monomers under alkaline conditions [25]. PDA materials display similar properties to natural melanins such as scavenging a variety of free radicals, rendering them with broad antioxidant biomedical applications [26]. Besides, PDA is easily deposited on the irregular surface of various substrates due to the strong chelating with mental materials [27,28]. For example, PDA-deposited microparticles prepared by  $MnCO_3$  template presented the broad-spectrum scavenging of ROS because of retaining a large amount of reductive phenolic hydroxyl group [29,30]. As a natural biopolymer, PDA shows its capability in scavenging ROS to treat many acute inflammatory diseases [31]. However, due to its unstable properties in harsh gastrointestinal environments, PDA for treating gastrointestinal diseases often needs to be combined with other materials for effective delivery to the disease site [32,33].

Herein, PDA-cladded montmorillonite micro-sheets (PDA/MMT) have been developed as a therapeutic platform for UC treatment. Both mucosal healing and broad-spectrum ROS scavenging are anticipated for the PDA/MMT platform (Fig. 1). More important, orally administrating PDA/MMT was expected to be transited to the inflamed gut where the inflammation occurred for UC patients. In this work, PDA was deposited on the surface of the exfoliated Na-MMT by the oxidative self-polymerization of dopamine under alkaline conditions. The preparation of PDA/MMT is a facile process, without any addition of toxic agents. A series of PDA/MMT has been fabricated by changing the depositing time or dopamine concentration during the oxidative polymerization depositing. Successes of PDA deposition on Na-MMT have also been carefully characterized by scanning electron microscope (SEM), energy dispersive spectrometer (EDS), and Fourier transform infrared spectroscopy (FTIR). Thereafter, the broad ROS-eliminating spectrum of PDA/MMT is carefully investigated by fluorescent probes. Moreover, the distribution of orally administrating PDA/MMT along intestinal tract was also evaluated by *in vivo* imaging. The therapeutic effect of PDA/MMT on murine ulcerative colitis model was investigated by monitoring colon length, body weight, histological appearance, and proinflammatory cytokines level. Finally, the therapeutic mechanism of PDA/MMT was probed in terms of inhibiting oxidative stress and repairing the gut mucosal barrier.

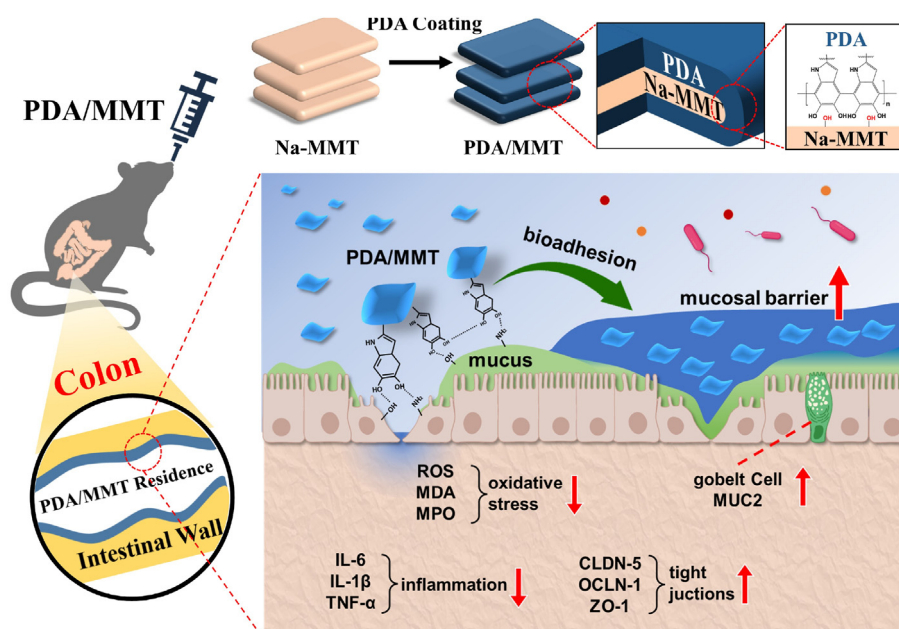


Fig. 1. Scheme of orally administered PDA/MMT micro-sheets for repairing the gut mucosal barrier.

## 2. Experimental methods and reagents

### 2.1. Materials and chemicals

Tris(hydroxymethyl)aminomethane, 3-Hydroxytyramine hydrochloride (dopamine), and medical-grade montmorillonite were purchased from Aladdin (Shanghai, China). Dextran sulfate sodium salt (DSS, 40 kDa) was purchased from Yeasen (Shanghai, China). 2,7-dichlorofluorescein diacetate (DCFH-DA) was purchased from Beyotime (Shanghai, China). 2,4,6-trinitrobenzene sulfonic acid solution (TNBS, 5% in H<sub>2</sub>O) was purchased from Sigma (Saint Louis, USA). SOD activity kit, DPPH scavenging kit, hydroxyl radical (•OH) scavenging kit, and superoxide anion (•O<sub>2</sub><sup>-</sup>) scavenging kit were purchased from Jiancheng (Nanjing, China). Heat-inactivated fetal bovine serum (FBS) and RPDA/MMT Medium 1640 were purchased from Thermo Fisher (Massachusetts, USA). Caco-2 cells were purchased from FuHeng Biology (Shanghai, China). ELISA kits of IL-6, IL-1β, and TNF-α were purchased from Jianglai (Shanghai, China).

### 2.2. Fabrication of PDA/MMT

The micro-sized Na-MMT sheet (Na-MMT) was first prepared by the previous methods with some modifications in studies [34,35]. Briefly, the naive Na-MMT powder (10 g) was firstly dispersed in 200 mL NaCl solution (0.1 M) for 24 h under stirring to obtain the coarse Na-MMT suspension, followed by washing with de-ionized water until free of chloride ions as tested by AgNO<sub>3</sub>. Thereafter, the coarse Na-MMT suspension was further exfoliated by two cycles of alternating probe ultrasound (300 W, 30 min) and bath ultrasound (80 W, 30 min). The unexfoliated components of the above dispersion were separated through centrifugation (2000 rpm, 15 min). The obtained supernatant was further centrifuged (12000 rpm, 15 min) to collect the exfoliated Na-MMT. Subsequently, depositing PDA polymer on the micro-sized Na-MMT sheet was carried out by oxidative polymerization of dopamine monomer in an alkaline condition according to the method in a previous study [36]. Briefly, the micro-sized Na-MMT sheet (3 g) was suspended in Tris(hydroxymethyl)aminomethane buffer (pH 8.5, 30 mL), followed by addition of dopamine monomer under stirring. The final concentration (4, 12, or 20 mg/mL) of dopamine monomer in the suspension was screened. After reaction for hours (2, 4, or 6 h), PDA/MMT paste was obtained by centrifugation at 12000 rpm and washed thrice times with de-ionized water for freeze-drying. Meanwhile, the free dopamine monomer in the supernatant was detected by measuring the absorbance at 280 nm. The deposited PDA amount for PDA/MMT was calculated by the following equation: PDA content = [(C<sub>i</sub> - C<sub>s</sub>) × V/W], where C<sub>i</sub> is the concentration of total dopamine input, C<sub>s</sub> is the concentration of dopamine in the supernatant; V is the total volume of suspension; W is the total weight of the solid Na-MMT amount.

### 2.3. SEM, EDS, and FTIR assay of PDA/MMT

The morphology of PDA/MMT powder was observed by using a HITACHI scanning electron microscope (SEM) (SU8010, HITACHI, Japan) at an acceleration voltage of 3 kV. The deposition of PDA was confirmed by Energy dispersive spectrometer (EDS, EX-350, HORIBA, Japan). Fourier transform infrared (FTIR) spectra were obtained by FTIR spectrometer (Gangdong, China) on KBr disc.

### 2.4. Scavenging reactive oxygen species

#### 2.4.1. Scavenging DPPH

DPPH kit as a typical radical was used to analyze the scavenging free radicals of PDA/MMT by the reported method [32]. DPPH solution (1.8 mL, 200 μM) was added to PDA/MMT suspension (0.1 mg/mL) and further incubated in dark. At different time (5, 10, 20, 30, 40, 60, 90, 120 min), UV-vis spectra of DPPH were real-time monitored and absorbance

at 515 nm was measured to calculate the DPPH radical scavenging activity based on the formula: radical scavenging activity =  $[1 - (A_t - A_b)/A_c] \times 100\%$ , where A<sub>c</sub> represents the absorbance of the blank solution without PDA/MMT; A<sub>t</sub> is the absorbance of the test sample after incubating with DPPH; A<sub>b</sub> is the absorbance of the test sample in 95% ethanol. To further determine the scavenging free radical efficacy of PDA/MMT, PDA/MMT suspension with varying concentrations (0.1, 0.2, 0.3, 0.4, or 0.5 mg/mL) was co-incubated with a certain amount of DPPH for 15min, followed by measuring absorbance at 515 nm and calculating scavenging radical activity. Three replicate samples were carried out for each test.

#### 2.4.2. Scavenging superoxide anion (•O<sub>2</sub><sup>-</sup>)

As a sensitive •O<sub>2</sub><sup>-</sup> indicator, NBT is reduced by •O<sub>2</sub><sup>-</sup> and forms blue formazan which presents the absorbance at 530 nm. The scavenging activity of superoxide anion (•O<sub>2</sub><sup>-</sup>) was determined by measuring the inhibition of NBT (nitro-blue tetrazolium) oxidation with a total SOD assay kit (Solarbio, China) according to the method in a previous study [37]. Briefly, PDA/MMT suspension (20 μL, 5 mg/mL) was incubated with SOD kits for 30 min at 37 °C, followed by detecting the absorbance at 530 nm. The scavenging activity of superoxide anion was calculated based on the following formula: radical scavenging activity =  $[(Ac1 - Ac2 - At)/(Ac1 - Ac2)] \times 100\%$ , where the absorbance of the test sample, positive SOD sample, and the reagent solution were denoted At, Ac1, and Ac2, respectively.

#### 2.4.3. Scavenging hydroxyl radical (•OH)

•OH is produced from H<sub>2</sub>O<sub>2</sub> in presence of Fe<sup>2+</sup> through the Fenton reaction. Scavenging activity of hydroxyl radical (•OH) was assessed by measuring the inhibition of Fe<sup>2+</sup> oxidation in according to the directions of the hydroxyl radical scavenging kit (Solarbio, China). 1,10-phenanthroline which can chelate to Fe<sup>2+</sup>, exhibits a concentration-dependent absorbance at 536 nm. Briefly, PDA/MMT suspension (150 μL, 0.5 mg/mL) was incubated with the hydroxyl radical scavenging kit for 60 min at 37 °C, followed by detecting the absorbance at 536 nm. The decrease of absorbance in presence of PDA/MMT presents the scavenging activity of •OH.

#### 2.4.4. Scavenging hydrogen peroxide (H<sub>2</sub>O<sub>2</sub>)

Scavenging activity of hydrogen peroxide (H<sub>2</sub>O<sub>2</sub>) is determined by a hydrogen peroxide detection kit (Solarbio, China). H<sub>2</sub>O<sub>2</sub> can react with titanium sulfate and form a yellow complex with characteristic absorption at 415 nm. After incubating PDA/MMT suspension (250 μL, 0.1 mg/mL) with the hydroxyl radical scavenging kit for 5 min at 25 °C, the absorbance at 415 nm was detected. The scavenging activity of H<sub>2</sub>O<sub>2</sub> was calculated by the following formula: scavenging activity of H<sub>2</sub>O<sub>2</sub> =  $(At - A0)/(Ac - A0) \times 100\%$ , where At is the absorbance in presence of PDA/MMT; Ac is the absorbance for the positive reagent; A0 is the absorbance of the blank reagent.

## 2.5. Cellular experiments

Human colonic epithelial cells (HT-29), human intestinal epithelial cells (Caco-2), and mouse macrophage cells (RAW 264.7) were cultured in a normal RPDA/MMT-1640 medium or DMEM supplemented with 10% heat-inactivated FBS and 1% penicillin/streptomycin at 37 °C in 5% CO<sub>2</sub> atmosphere and 70% relative humidity, respectively.

### 2.5.1. Cell viability assay

Caco-2, HT-29, or RAW 264.7 cells were seeded at a density of 5 × 10<sup>3</sup> cells per well in 96-well plates (Corning, USA) for 24 h for attachment and then cultured with PDA/MMT or Na-MMT at various concentrations (0.125, 0.25, 0.5, 0.75, 1.0, 1.5 mg/mL) for 24 h. Afterward, the relative cell viability was detected by the standard methyl thiazolyl tetrazolium (MTT) assay. In addition, Calcein AM/propidium iodide (PI) staining was carried out to determine the live/dead cells.

### 2.5.2. Scavenging cellular ROS

Caco-2 cells were seeded at a density of  $1 \times 10^4$  cells per well in 12-well plates for 24 h and then cultured with PDA/MMT or Na-MMT (1 mg/mL) in presence of  $\text{H}_2\text{O}_2$  (1000  $\mu\text{M}$ ) for 10 h. The intracellular ROS levels were detected by the 2',7'-dichlorofluorescein-diacetate (DCFH-DA) (Beyotime, China) fluorescent dye [32]. All the images were acquired by an inverted fluorescent microscope (Nikon ECLPSE TS2, Japan).

## 2.6. In vivo animal experiments

### 2.6.1. Gut distribution of orally administrating PDA/MMT

Na-MMT sheet and PDA coating for PDA/MMT were first labeled with FITC and DIL, respectively. After orally administrating fluorescence-labeled PDA/MMT suspension (0.2 mL, 40 mg/mL), the mice were sacrificed to harvest the guts and immediately imaged by IVIS imaging (IVIS Lumina II, Ex = 495 nm, Em = 519 nm). Meanwhile, the fresh colons were frozen, sectioned, and stained with DAPI to detect the fluorescence distribution of colon mucosa by Nikon confocal laser scanning microscopy (Nikon ECLPSE Ti2, Japan). The fluorescence intensity for at least 10 horizons in each sample was measured by using the computer-assisted analysis method (Image J analysis software).

### 2.6.2. DSS-induced ulcerative colitis in mice

C57BL/6 mice (Male, 6–8 weeks) were purchased from the Laboratory Animals Centre of Wenzhou Medical University. All the animals were maintained in the SPF care facility, fed with sterilized mice chow pellets, and drinking water supplied in bottles under a 12 h light/dark cycle. The animals were allowed to acclimatize at least 7 days before experiments. Animal experiments were strictly carried out according to the guidelines issued by the Institutional Animal Care and Use Committee of Wenzhou Medical University.

For the establishment of the colitis model, the mice were given drinking water containing 3.5% DSS (44 kDa) ad libitum for 7 consecutive days. DSS-induced mice with ulcerative colitis were divided into three groups: DSS group (saline,  $n = 6$ ), Na-MMT (3.9 mg/10 g), and PDA/MMT (3.9 mg/10 g), respectively ( $n = 6$ ). Normal mice without DSS treatment were given saline for control. PDA/MMT or Na-MMT powder was homogeneously dispersed in water to form a stable suspension. PDA/MMT or Na-MMT suspension (0.2 mL each mouse) was orally administered once a day for each treatment since the 5<sup>th</sup> day. During the treatments, the colon of mice 1–3 cm away from the anus in each group was imaged by the small animal endoscope (ShenDa, China). Besides, the disease activity index (DAI) of mice in each group was monitored every day. DAI score was based on the summation of five parameters: stool consistency, weight loss, rectal bleeding, food, and water intake, and the mental state of the mice, which were depicted in previous studies [38]. At the endpoint, the mice were sacrificed to collect colons and the colonic length was determined.

### 2.6.3. Histological morphology

The colon slices were stained with hematoxylin and eosin (H&E) to investigate the morphology of colons and the histological scores were performed according to the previous studies [39,40]. For further histological examinations, the deparaffinized sections were stained with Alcian Blue Periodic acid Schiff (AB-PAS), and Masson Trichrome (Masson). Finally, the histological morphology of the colon was observed under a Nikon microscope (Nikon ECLPSE 80i, Japan). Goblet cells were observed by immunofluorescence staining of cytokeratin 18 (CK18) and Mucin 2 (MUC2). The sections of colons were stained with mouse monoclonal cytokeratin 18 (10830-1-AP, 1:500, Proteintech®), rabbit polyclonal mucin 2 (DF8390, 1:200, Affinity®), followed by fluorescent secondary antibody conjugated with CoraLite488 (SA00013-1, 1:200, Proteintech®) or Rhodamine (BS10250, 1:200, bioworld®). MUC2<sup>+</sup>CK18<sup>+</sup> staining was regarded as goblet cells with secretory activity [41].

### 2.6.4. Histological staining of pro-inflammatory cytokines

The colon sections were treated with 0.3% hydrogen peroxide containing methanol at 37 °C for 10 min, boiled in EDTA-Tris buffer at pH 9.0 for 5 min for antigen retrieval, and blocked with 5% BSA in PBS with 0.1% Tween 20 (PBST). The colon samples were then incubated with primary antibodies overnight. The primary antibodies included: IL-1 $\beta$  (ab9722, 1:200, Abcam®), mouse monoclonal TNF- $\alpha$  (60291-1-Ig, 1:400, Proteintech®), mouse polyclonal IL-6 (66146-1-Ig, 1:400, Proteintech®), rabbit polyclonal MCP-1 (ab7202, 1:200, Abcam®), mouse monoclonal CD206 (sc-58986, 1:200, santa cruz®), CD80 (bs-2211R, 1:200, Bioss®), and rabbit polyclonal myeloperoxidase (ab208670, 1:500, Abcam®). After washing with PBST, the sections were incubated with goat anti-rabbit or goat anti-mouse IgG H&L (HRP) secondary antibodies, which were then identified by a DAB chromogen kit (ZSGB-BIO, Beijing, China). Histological evaluation was then performed on a Nikon microscope (Nikon ECLPSE 80i, Japan). At least 4 representative areas were photographed to analyze, and the proportion of positively stained cells was then measured by the computer-assisted analysis method (Image J analysis software).

### 2.6.5. ELISA assay of IL-1 $\beta$ , IL-6 and TNF- $\alpha$

IL-1 $\beta$  and IL-6, and TNF- $\alpha$  in colon homogenate were quantified by enzyme-linked immunosorbent assay (ELISA) by using commercial mice IL-6 (JL20268, jianglai, China), IL-1 $\beta$  (JL18442, jianglai, China), and TNF- $\alpha$  ELISA kit (JL10484, jianglai, China). The colon was weighed and homogenized in 4 °C RIPA lysis buffer (P0013B, Beyotime, China), and the supernatant was collected for evaluation. The final result of the ELISA test is the ratio of the pro-inflammatory protein concentration to the corresponding total protein concentration (pg/mg protein) determined using commercial BCA kits (20201ES76, Yeasen, China).

### 2.6.6. Detecting tight junctions

For immunofluorescence staining, the colon sections were stained with rabbit polyclonal occludin (ab216327, 1:200, Abcam®), rabbit polyclonal claudin-5 (A10207, 1:100, ABclonal®), and rabbit polyclonal ZO-1 (A0659, 1:200, ABclonal®) for 12 h in 4 °C followed by secondary antibody conjugated with CoraLite488 (SA00013-1, 1:200, Proteintech®) or Rhodamine (BS10250, 1:200, bioworld®). The nuclei were stained with an anti-fluorescent quenching mountant containing DAPI (36308ES11, Yeasen®). All the fluorescent images were obtained by using a Nikon confocal laser scanning microscopy (Nikon ECLPSE Ti2, Japan).

For Western blot, antibodies of rabbit polyclonal occludin (27260-1-Ig, 1:2000, Proteintech®), rabbit polyclonal claudin-5 (A10207, 1:1000, ABclonal®), mouse monoclonal ZO-1 (sc-374221, 1:1000, Santacruz®), rabbit recombinant  $\beta$ -actin (81115-1-RR, 1:5000, Proteintech®) and rabbit polyclonal GAPDH (10494-1-AP, 1:10000, Proteintech®) were used. The blots of protein were finally visualized using Super-Signal West Femto Chemiluminescent Substrate (Thermo Scientific, USA).

### 2.6.7. Detecting oxidative stress

The fresh colon was frozen, sectioned, and incubated with 2,7-dichlorofluorescein diacetate (DCFH-DA) at 37 °C for 20 min to detect ROS level. Besides, the activity of superoxide dismutase (SOD), malonaldehyde (MDA), and myeloperoxidase (MPO) in the colon homogenate were measured by the commercial SOD kit (BC0170, Solarbio, China), MDA kit (BC0025, Solarbio, China), and mice MPO kit (A044-1-1, Jiancheng, China).

## 2.7. Statistical analysis

Data were expressed as the mean  $\pm$  standard deviation of at least three independent replicates. The student t-test was performed for comparisons between the two groups. The one-way ANOVA was performed for multiple groups. Pearson's  $r$  and the P values were determined by simple linear regression.

### 3. Results and discussions

#### 3.1. Preparation and characterization of PDA/MMT

Na-MMT presents the superior dispersity and long-term colloidal stability due to the reduced charge inside its layered sheets [21,42].  $\text{Ca}^{2+}$

of the naive MMT was first substituted with  $\text{Na}^+$  to prepare Na-MMT, followed by ultrasonic treatment for the exfoliation of micro-sized Na-MMT. Truly, the exfoliated Na-MMT was homogeneously dispersed in water for several hours without settling (Fig. S1). PDA/MMT was fabricated by depositing PDA on the surface of exfoliated Na-MMT (Fig. 2A). The self-oxidative polymerization of dopamine made PDA

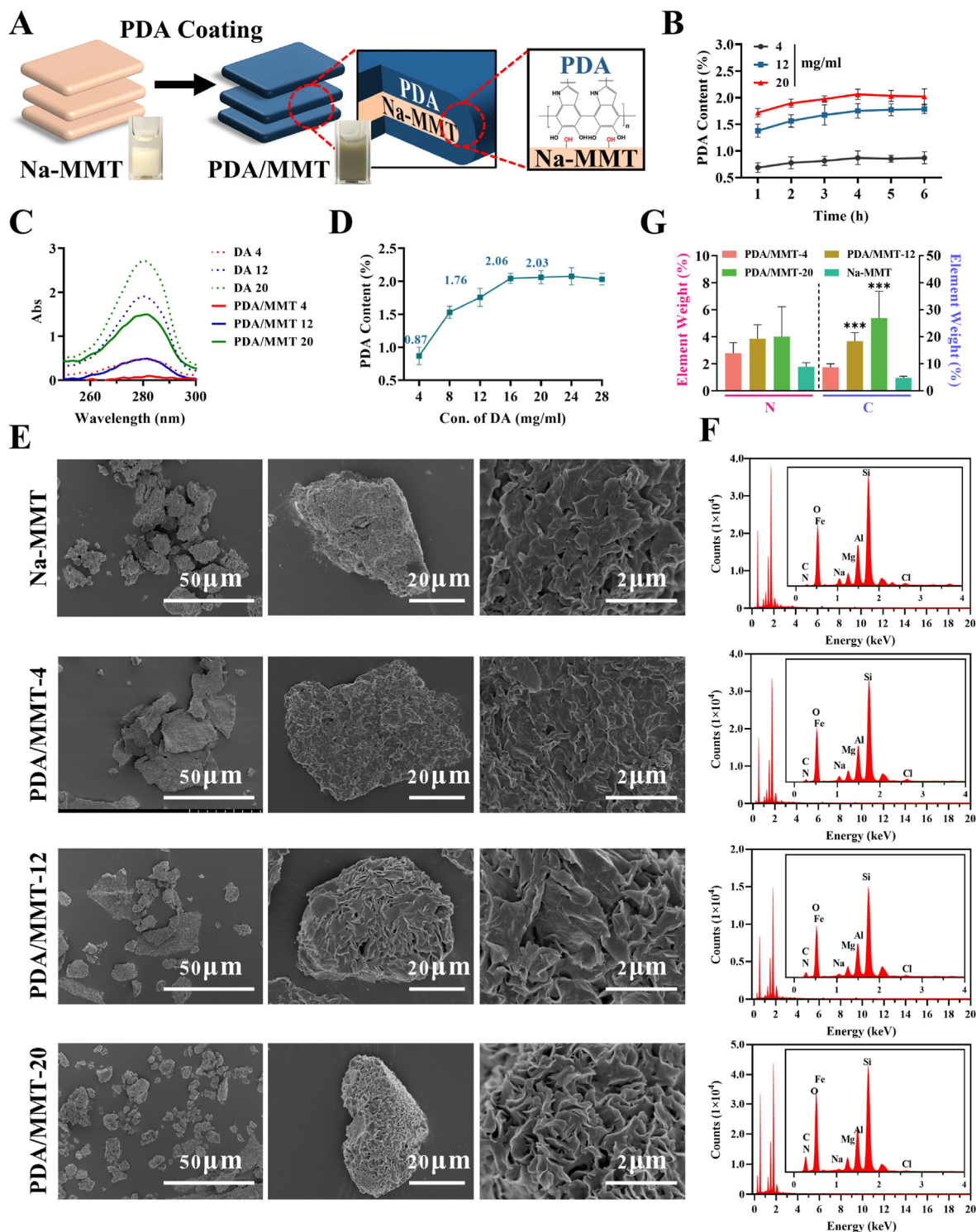


**Fig. 2.** Preparation and characterization of PDA/MMT. (A) Schematic of exfoliation of Na-MMT and *in situ* self-oxidative polymerization of dopamine onto Na-MMT. (B) The PDA content of PDA/MMT after varying polymerization time. (C) UV-vis absorption spectra of DA solution of different concentration (DA 4, 12, 20) and corresponding primal supernatant of the reaction after DA deposition (PDA/MMT 4, 12, 20). (D) The PDA content of varying dopamine concentration during polymerization. (E) SEM image and (F) corresponding EDS of freeze-dried Na-MMT and PDA/MMT. (G) Quantitative statistics of element weight percentage from EDS (\*\*P < 0.001, \*\*P < 0.01, \*P < 0.05, n ≥ 3).

deposit on the surface of the irregular substrate in a slightly basic medium (pH 8.5). Both the deposition time and the dopamine concentration were two key factors to determine the thickness of PDA coating of PDA/MMT. Results were shown in Fig. 2B–D. PDA deposition was very fast and the plateau was usually approaching within 4 h for each tested concentration of dopamine (Fig. 2B). At 4 h, the obvious decrease of free dopamine in the supernatant was indicated by the absorption at 280 nm (Fig. 2C), suggesting the effective deposition of PDA. It has been reported that the deposited PDA film can become unstable and completely detached from the substrate when the depositing time occurs for a prolonged period [26]. The deposited PDA amount per gram of Na-MMT for PDA/MMT sheet was dependent on the concentration of dopamine monomer. The deposited PDA amount was linearly increasing within 4–16 mg/mL of dopamine monomer. Excess of dopamine monomer did not increase PDA depositing. The deposited PDA plateau was reaching to  $2.06 \pm 0.08\%$  when the concentration of dopamine was 20 mg/mL (Fig. 2D). *In situ* deposition of PDA is an oxidative polymerization, which is constrained by oxygen in the medium [25]. PDA/MMT with various PDA deposition (0.8%, 1.7%, and 2.0%) was fabricated by controlling dopamine concentrations of 4, 12, and 20 mg/mL (PDA/MMT-4, PDA/MMT-12, and PDA/MMT-20) for the following studies.

The dried Na-MMT was white powder while PDA/MMT product became black (Fig. 2A). The morphology of PDA/MMT was observed by SEM, and the results were shown in Fig. 2E. PDA/MMT presents the similar sheet-like shape as Na-MMT, while their surface became coarser due to PDA deposition. Furthermore, PDA coating on the surface of PDA/MMT became denser as the deposited PDA amount increased. PDA/MMT was further detected by EDS. Na-MMT presents the composed elements (Si, Al, Mg, and Na), which is exactly consistent with that in the previous study. Besides the composed elements, the new elements including N and C were also detectable in PDA/MMT (Fig. 2F/G). Moreover, the counts of N and C elements for PDA/MMT were rising with the increase of the deposited PDA amount. PDA coating was further characterized by FT-IR spectrums. As shown in Fig. S2, the typical vibrating peaks of N–H ( $3420, 3250 \text{ cm}^{-1}$ ) and C=C ( $1530, 1630 \text{ cm}^{-1}$ ) were clearly observed for PDA/MMT. Moreover, groups of new peaks at  $1350 \text{ cm}^{-1}$  attributed to the indole ring, which was not observed in DA, were detectable in PDA/MMT. Oxidative polymerization of dopamine into PDA is involved in forming self-assembled trimer of (dopamine)<sub>2</sub>/5,6-dihydroxyindole, which is similar to the mechanism for synthetic melanin synthesis [43]. These results confirmed the success of PDA coating on the surface of MMT.

### 3.2. *In vitro* broad-spectrum ROS scavenging of PDA/MMT

PDA polymer with a large amount of phenolic hydroxyl possesses the broad-spectrum ROS scavenging via proton transfer or electron transfer [29,44,45]. ROS scavenging activity of PDA/MMT toward varieties of ROS sources was investigated by using DPPH probe and results were displayed in Fig. 3A/B. DPPH is a stable free radical, presenting the maximum UV absorbance at 515 nm. The absorption of DPPH was obviously decreasing after incubating with PDA/MMT while the negligible change was observed for Na-MMT treatment. Moreover, the DPPH scavenging ability was dependent on the PDA content of various types of PDA/MMT. As high as 80% and 90% of DPPH was scavenged by PDA/MMT-12 and PDA/MMT-20, respectively. DPPH scavenging capacity of PDA/MMT-20 was approximately eight times that of Na-MMT at the same concentration. Besides, the concentration-dependent removing profiles was also observed for these PDA/MMT sheets (Fig. 3C). The speed of scavenging free radicals is also important for an effective ROS scavenging material. The time-dependent DPPH scavenging was investigated for PDA/MMT sheets. As shown in Fig. 3D, DPPH scavenging was very fast and the plateau was reaching within 30 min for PDA/MMT. Especially, nearly 80% of DPPH was scavenged by PDA/MMT-20 at the concentration of 0.3 mg/mL, indicating its high efficiency of scavenging free radicals. However, the scavenging speed for

ROS-scavenging materials in previous study are too slow such that approximately 8 h was required for effectively scavenging ROS [46].

•OH is another detrimental source of highly oxidizing ROS and the specific enzyme eliminating •OH is of lack in biological body. •OH scavenging of PDA/MMT was also detected and results was displayed in Fig. 3E/F. PDA/MMT also present the good scavenging ability of •OH. Interestingly, the •OH scavenging ability of Na-MMT seem be comparable to that of PDA/MMT. This was due to the fact that •OH, one of the most active free radicals, can react with numerous reactive sites of Na-MMT [47]. Besides, the exfoliated Na-MMT micro-sheet with huge specific surface area and numerous reactive sites have also led to the high potential of scavenging •OH [24,48].

SOD-like activities of PDA/MMT were further assessed by scavenging •O<sub>2</sub><sup>-</sup> and results were shown in Fig. 3G. Xanthine (X) could generate •O<sub>2</sub><sup>-</sup> in presence of xanthine oxidase (XO), which produce a purple oxidative substance. About 80% of the produced •O<sub>2</sub><sup>-</sup> was scavenged for PDA/MMT at the test concentration. Whereas only 30% of the produced •O<sub>2</sub><sup>-</sup> was scavenged by Na-MMT at the comparable dose. H<sub>2</sub>O<sub>2</sub> can react with titanium sulfate and form a yellow complex. The H<sub>2</sub>O<sub>2</sub> scavenging ability of PDA/MMT was also detected and results were shown in Fig. 3H. PDA/MMT presented the more obvious H<sub>2</sub>O<sub>2</sub> scavenging than Na-MMT. Moreover, the PDA-dependent scavenging ability was also observed for various types of PDA/MMT. H<sub>2</sub>O<sub>2</sub> scavenging is of great importance, as H<sub>2</sub>O<sub>2</sub> presents the indiscriminate reactivities and is a intermediate of ROS metabolism [44,49]. Some antioxidative enzyme-based materials promote H<sub>2</sub>O<sub>2</sub> decomposition without taking •OH generation into account [49]. Collectively, these results indicated that PDA/MMT have the broad-spectra of scavenging ROS.

### 3.3. Cellular protective ability of PDA/MMT against oxidative stress

To further verify the ROS scavenging capacity of PDA/MMT *in vitro*, it was applied to scavenge the intracellular ROS of colonic epithelial cells (Caco-2 cells). The intracellular ROS levels of Caco-2 cells were detected by the 2',7'-dichlorofluorescein-diacetate (DCFH-DA) fluorescent dye (Fig. 4A). The fluorescence of DCF showed a significantly increased ROS level in Caco-2 stimulated with Rosup, which elevates intracellular ROS levels directly [31]. Both PDA/MMT and Na-MMT incubation led to the elimination of intracellular ROS and the maximal elimination was observed in the PDA/MMT-20. Interestingly, the intracellular ROS scavenging efficiency of PDA/MMT also showed a positive correlation with PDA content (Fig. 4B). The nonspecific toxicity of PDA/MMT or Na-MMT toward epithelium was analyzed by using MTT assay, where 89.3% and 108.6% of viability were preserved for cells treated with Na-MMT and PDA/MMT for 24 h, respectively. Similar results were also obtained on HT-29 cells and RAW 264.7 (Fig. S3). Herein, both PDA/MMT and Na-MMT from 0.12 mg/mL to 1.5 mg/mL caused the negligible cytotoxicity, indicating the high biocompatibility of MMT-based materials (Fig. 4C/D).

After confirming the *in vitro* ROS scavenging activity of PDA/MMT, its cell protective property against oxidative stress in cells was investigated. ROS-mediated oxidative stress is a key mediator in the pathogenesis and progression of UC [50]. H<sub>2</sub>O<sub>2</sub> can elevate the intracellular ROS level of Caco-2 cells, simulating the oxidative stress imbalance within cells. The cell viability of Caco-2 cells incubated with a high concentration of H<sub>2</sub>O<sub>2</sub> significantly decreased. Whereas, the cell viability was significantly improved by PDA/MMT treatment (1 mg/mL) in the certain concentration of H<sub>2</sub>O<sub>2</sub> (Fig. 4E). ROS and oxidative stress affect apoptosis via regulating numerous protein kinase cascades [51,52]. We assumed that PDA/MMT treatment improve the cell viability via preventing ROS-induced apoptosis. Therefore, the intracellular ROS were detected by DCFH-DA, and the corresponding apoptosis situation was examined through calcein AM/propidium iodide (AM/PI) staining. Results were showed in Fig. 4A. H<sub>2</sub>O<sub>2</sub> stimulation significantly enhanced intracellular ROS levels and caused obviously the cellular apoptosis simultaneously. By contrast, PDA/MMT treatment effectively relieved oxidative stress

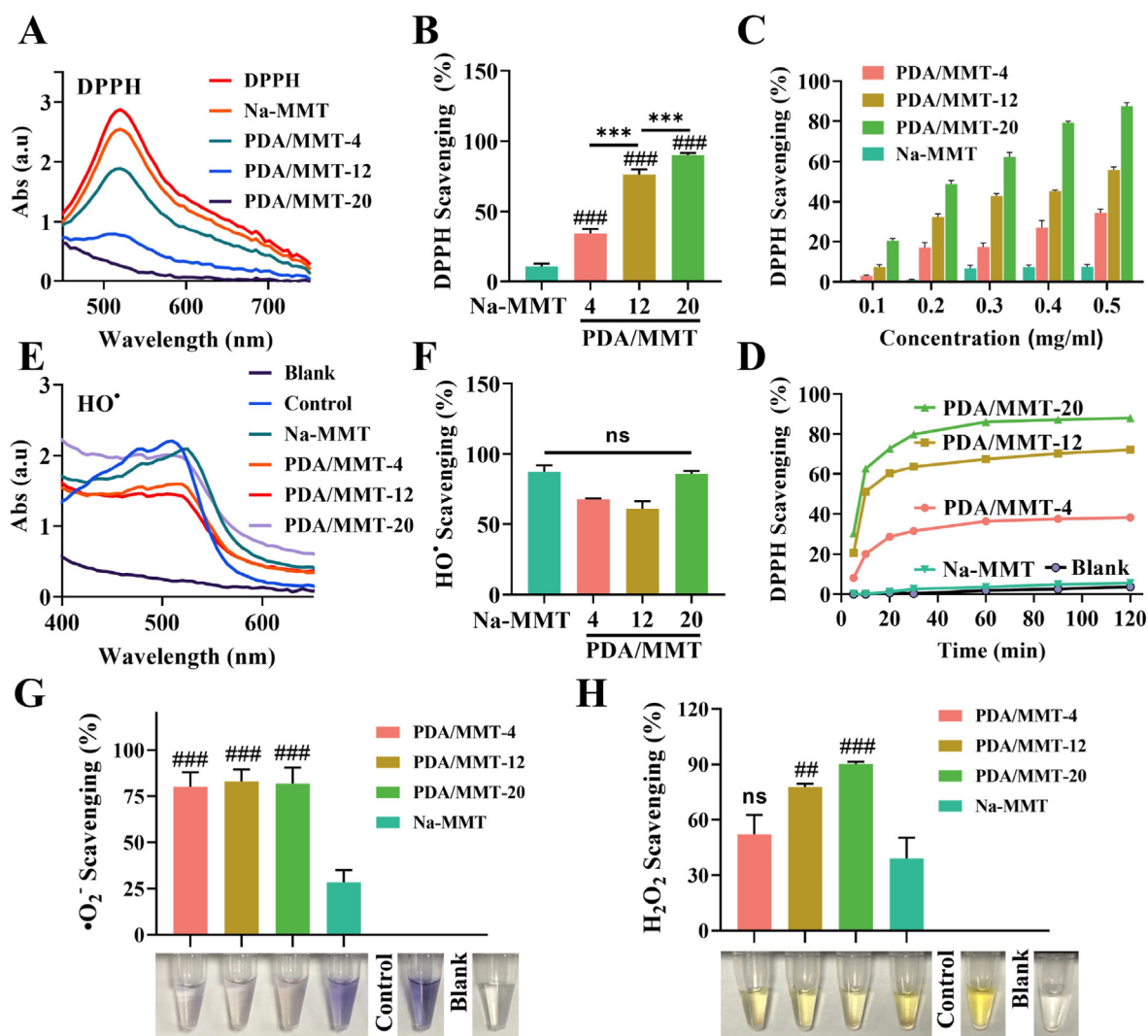


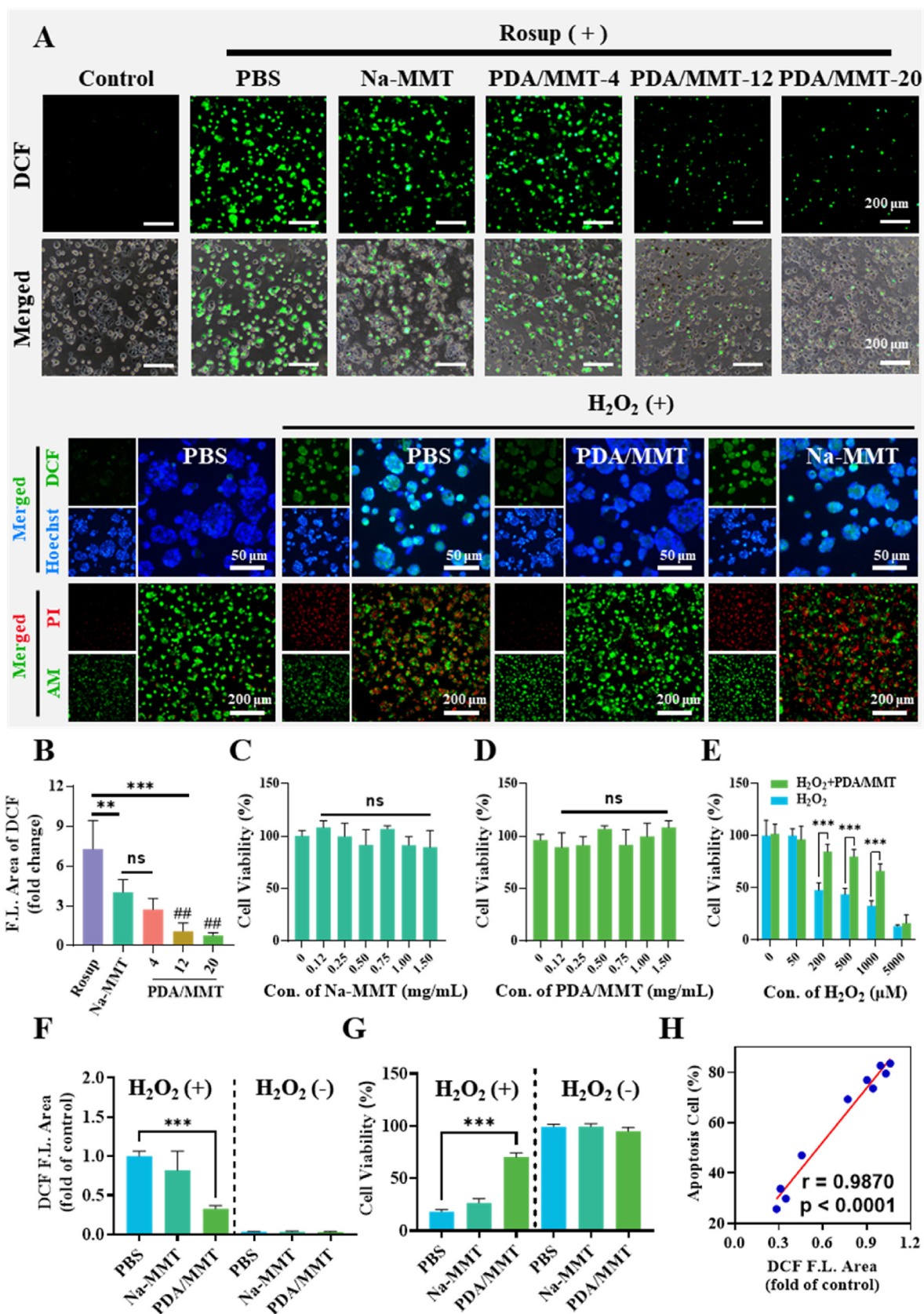
**Fig. 3.** ROS scavenging activities of PDA/MMT. (A) UV-vis absorption spectra of DPPH solution. (B) DPPH scavenging ratio calculated from UV-vis absorbance at 515 nm. (C) DPPH scavenging percentage of PDA/MMT and Na-MMT at varying concentrations. (incubation time = 10 min). (D) Kinetic curves of DPPH scavenging of PDA/MMT and Na-MMT (concentration = 0.3 mg/mL). (E) UV-vis absorption spectra of hydroxyl radical solution. (F) Hydroxyl radical scavenging ratio calculated from UV-vis absorbance at 560 nm. (G) Superoxide anion scavenging ratio calculated from UV-vis absorbance at 530 nm. (H)  $\text{H}_2\text{O}_2$  scavenging ratio calculated from UV-vis absorbance at 415 nm (\*\* $P < 0.01$ , \* $P < 0.05$ ; and ### $P < 0.001$ , ## $P < 0.01$ , # $P < 0.05$ ,  $n \geq 3$ , vs Na-MMT).

and abolished the cellular apoptosis correspondingly (Fig. 4F/G). Intracellular ROS level was positively correlated with the apoptosis of Caco-2 cells, which may explain the protective effect of PDA/MMT (Fig. 4H). Similarly, PDA/MMT treatment also exhibit protection against apoptosis of LPS-induced oxidative stress (Fig. S4). In summary, PDA/MMT relieved oxidative stress-induced apoptosis through scavenging ROS, and offered the better protection than Na-MMT as antioxidants.

### 3.4. Gut distribution of PDA/MMT after oral administration

In order to track the orally administrated PDA/MMT in gut, Na-MMT micro-sheet and PDA coating was labeled with FITC and DIL, respectively. The distribution and retention of the fluorescent PDA/MMT was observed by IVIR imaging. The solution dissolving FITC and DIL (FITC&DIL) or FITC-labeled Na-MMT (FITC-MMT) was used as control and its distribution in gut was also detected. Results were shown in Fig. 5A. The fluorescence of FITC&DIL was rapidly transited to the caecum at 1.5 h after oral administration, followed by the rapid clearance within 4 h. By contrast, the retention of FITC-MMT in the small intestine was much longer than that of FITC&DIL, and it took at least 4 h to reach the colon. This was due to the mucoadhesive property of MMT *in vitro*

[23]. However, FITC-MMT was not effectively remained at colon, and was rapidly excreted along with feces. No obvious fluorescence of FITC-MMT was observed at 6 h. The orally administrated PDA/MMT was residing in stomach for about 1–2 h, followed by emptying to the small intestine. At 6 h, few of orally administrated PDA/MMT was accumulated in the small intestine, and most of them was distributed in the colon. Moreover, PDA/MMT tightly adhere to the whole colon within 4 h, and remained in the distal colon for a long time (Fig. 5B). The fluorescence signal in the colon was about 5 times higher than that of FITC-MMT or liquid after oral administration for 6 h (Fig. 5C). Alternatively, the distal colon tissues were sectioned and further observed using confocal laser scanning microscope (CLSM). In line with the result of *ex vivo* imaging, no fluorescence signal was observed in distal colon for FITC&DIL at 6 h, and there was only weak fluorescence inside colon section for FITC-MMT group. Whereas, PDA-MMT group showed the obvious fluorescence in colon sections. Moreover, the fluorescence of PDA was coincided with that of FITC-MMT, indicating that the enhanced adhesion of PDA/MMT was caused by PDA. After subjecting them to the simulated gastric fluid (SGF, pH 1.2) for 1 h, the stability of PDA/MMT has been carefully investigated by SEM and EDS imaging. Results of SEM and EDS analysis showed that the morphology and the element composition of PDA/MMT



(caption on next page)

**Fig. 4.** Cellular protective ability of PDA/MMT against oxidative stress. (A-1) DCF fluorescence and bright field image of Caco-2 cells incubated with Rosup and PDA/MMT or Na-MMT. (A-2) Fluorescent images of Caco-2 cells stained with DCFH-DA (green, intracellular ROS) after various treatments as indicated. Fluorescent images of Caco-2 cells stained with Calcein-AM (green, live cells) and propidium iodide (red, dead cells) after treatments.  $H_2O_2$  concentration is 500  $\mu M$  in those two experiments. (B) Quantitative statistics of DCF fluorescence area ratio from Fig A1. (C) Cell viability of Caco-2 incubated with varying concentrations of Na-MMT after 24 h. (D) Cell viability of Caco-2 incubated with varying concentrations of PDA/MMT after 24 h (E) Cell viability of Caco-2 incubated with  $H_2O_2$  (0–5000  $\mu M$ ),  $H_2O_2$  plus PDA/MMT (1 mg/mL) after 24 h. (F) Fold change of DCF fluorescence area compared to control ( $H_2O_2$ +PBS) from Fig A2. (G) Cell viability of Caco-2 after various treatments as indicated in Fig A2. (H) Correlation plots comparing the apoptosis to the corresponding intracellular ROS level (DCF fluorescence area). Pearson's r and the P values were determined by simple linear regression (\*\* $P < 0.001$ , \* $P < 0.01$ , \* $P < 0.05$ ,  $n \geq 3$ ). (For interpretation of the references to color in this figure legend, the reader is referred to the Web version of this article.)

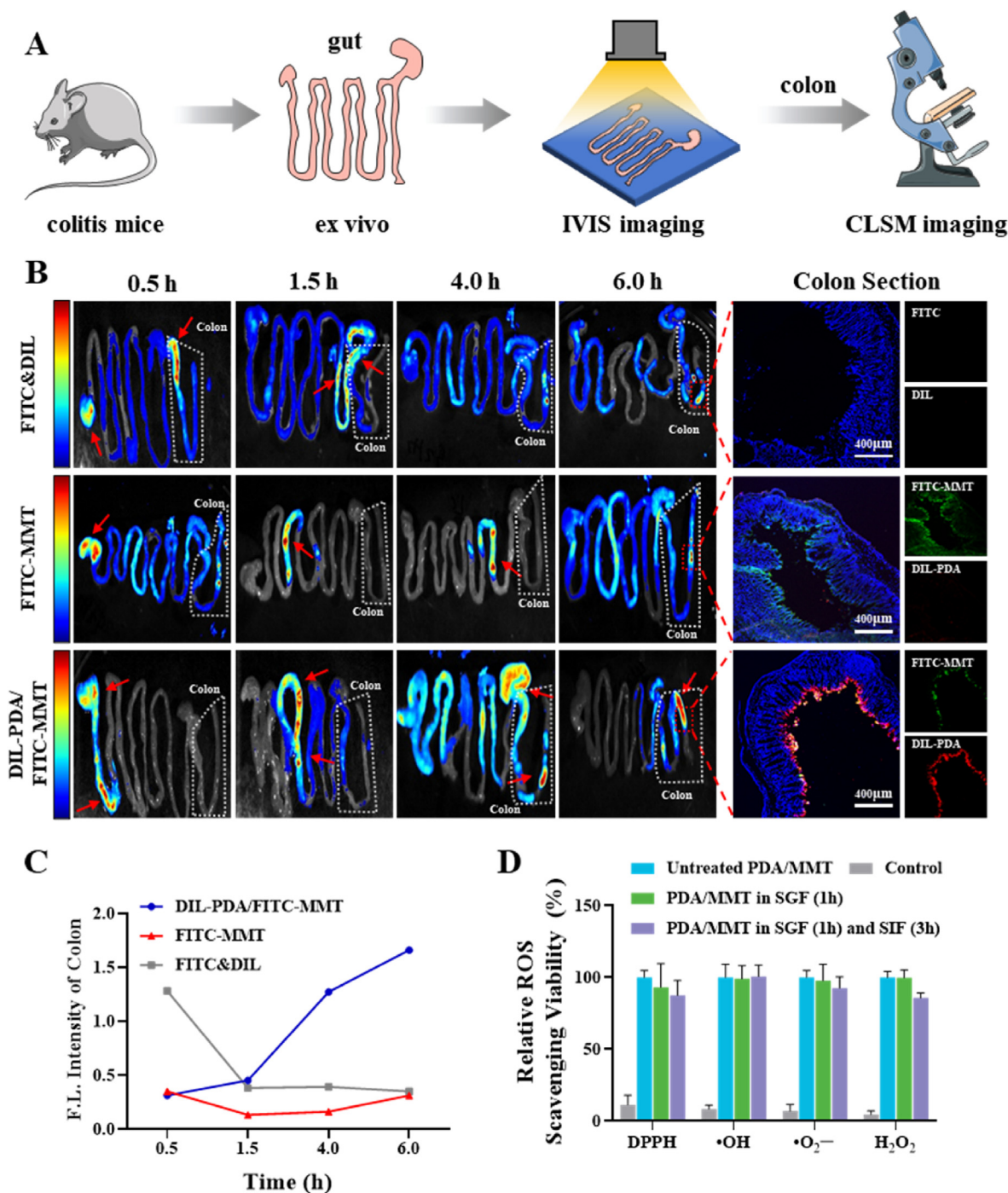


**Fig. 5.** Gut distribution of orally administrated PDA/MMT. (A) Schematic of ex vivo imaging of gut using IVIS system, and corresponding confocal laser scanning microscope (CLSM) imaging of colon sections. (B) The ex vivo imaging of gut of different groups at 0.5, 1.5, 4, and 6 h after oral administration, and corresponding CLSM imaging of colon sections. (C) fluorescence intensity of colon. (D) Relative ROS scavenging viability of PDA/MMT treated with simulated gastric fluid (SGF) for 1 h and simulated intestinal fluid (SIF) for 3 h.

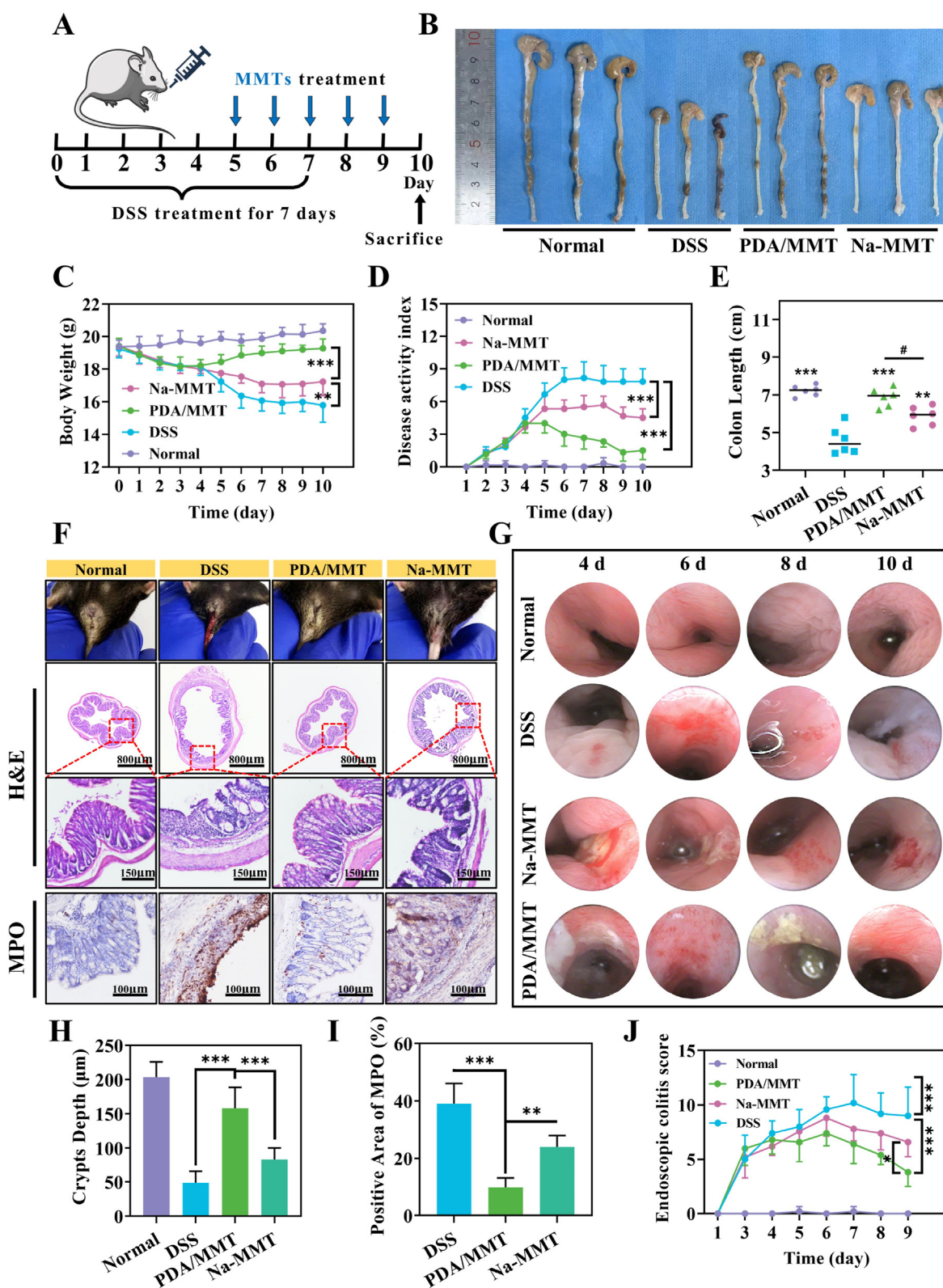


**Fig. 6.** PDA/MMT ameliorated DSS-induced ulcerative colitis. (A) Schematic of the procedure of mice colitis establishment and treatment. (PDA/MMT and Na-MMT are collectively termed as MMTs) (B) Digital photographs of colons and (E) corresponding colon length (C) Body weights of different groups of mice over 10 days. (D). Disease activity index (DAI) of mice over 10 days (F-1) Digital photographs of excretion and bleeding of mice at day 10. (F-2) H&E staining of transverse sections of mice colon. (F-3) Immunohistochemical staining of myeloperoxidase (MPO) of transverse sections of mice colon and (I) corresponding positive area of MPO (H) Crypt depth calculated from H&E staining. (G) Digital photographs of colons were imaged by small animal endoscope and (J) endoscopic colitis score based on endoscopic image. (\*\* $P < 0.001$ , \*\* $P < 0.01$ , \* $P < 0.05$ ,  $n \geq 3$ ).

after SGF incubation was similar to that of its origin form (Fig. S6 and Fig. 2E). The retention of PDA on PDA/MMT after incubating with SGF was further confirmed by FT-IR analysis. The typical peaks of PDA, including the N-H vibrating ( $3420, 3250\text{ cm}^{-1}$ ) and the C=C vibrating ( $1530, 1630\text{ cm}^{-1}$ ), were still observed for PDA/MMT after SGF treatment (Fig. S7). Moreover, the remaining ROS scavenging viability of PDA/MMT after 1 h of incubating with SGF was more than 90% of the untreated PDA/MMT (Fig. 5D). Even further subjecting to the simulated intestinal fluid (SIF) for 3 h, more than 85% of ROS scavenging viability of PDA/MMT was still preserved (Fig. 5D), indicating the ROS-scavenging viability of PDA/MMT transited to colon was not greatly compromised. Altogether, the above findings suggested that SGF treatment neither disturb the structure of PDA/MMT nor significantly destroy PDA coating after incubating with SGF.

### 3.5. PDA/MMT ameliorated DSS-induced ulcerative colitis

*In vivo* therapeutic efficacy of PDA/MMT was investigated on DSS-

induced mouse UC models. Fig. 6A summarizes the overall experimental procedure, and the physiological state of mice were thoroughly recorded and analyzed to investigate the therapeutic effect of PDA/MMT. Orally administrated PDA/MMT effectively ameliorate the colitis-associated symptoms of murine model. DSS-induced colitis result in great drop in body weight and colon length, and increased DAI within 10 days, indicating the successful establishment of ulcerative colitis. PDA/MMT treatment induced a significant improvement in these indicators, while Na-MMT did not produce the obvious improvement (Fig. 6B-E). In addition, the colonic mucosa of mouse was further assessed by a small animal endoscope in term of the ulceration, vascular pattern, hyperemia, visible fibrin, and rectum stenosis. Results were showed in Fig. 6G/J. The colonic mucosa of mouse in Na-MMT group were pale and presented the bleeding ulcers during the whole process. However, these parameters were significantly improved in mice treated with PDA/MMT. Moreover, on the 10<sup>th</sup> day after PDA/MMT treatment, the morphology of colonic mucosa was recovered to the comparable level of healthy colon in normal group.

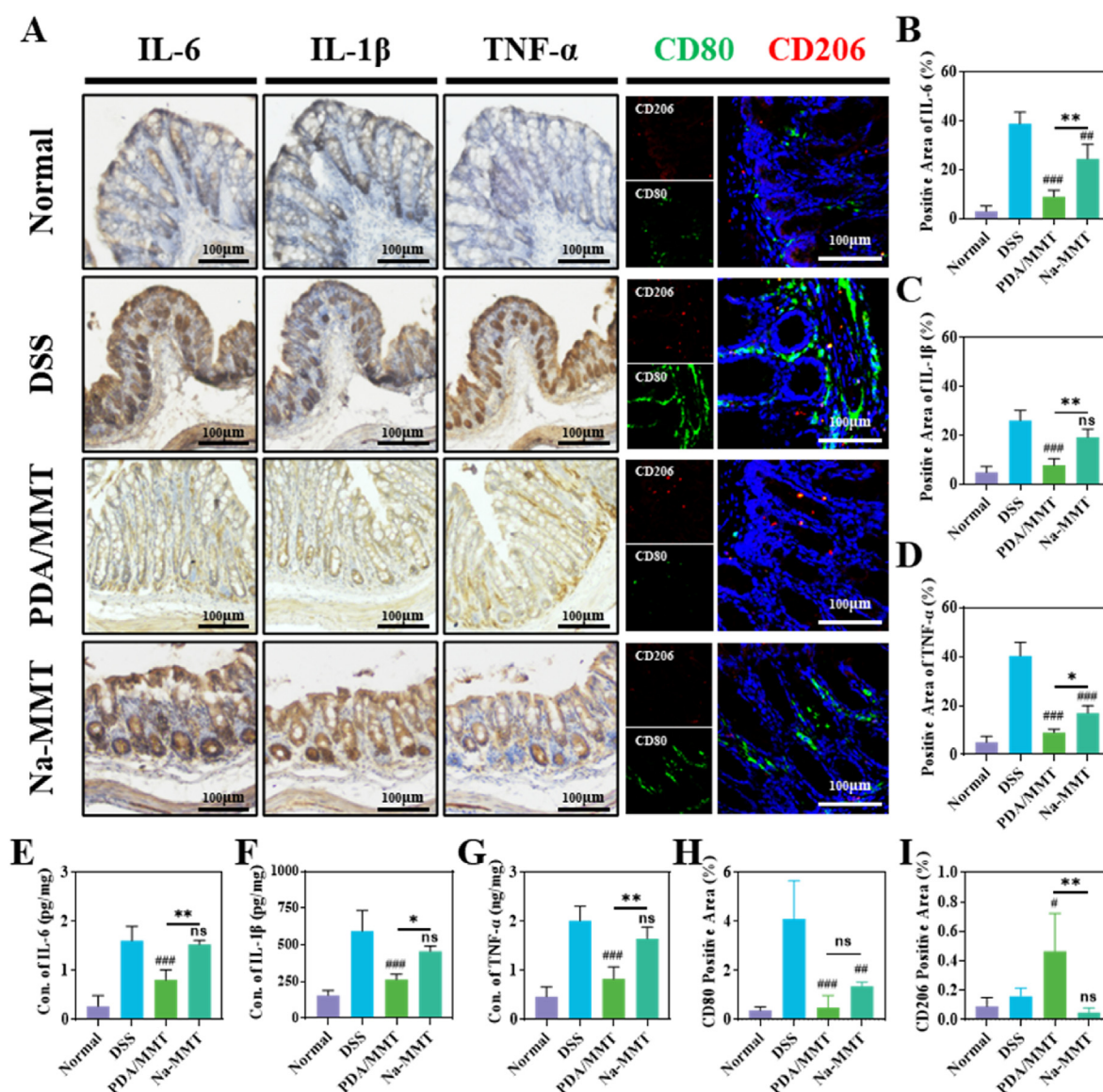


**Fig. 7.** PDA/MMT alleviated inflammatory response of ulcerative colitis. (A-1) Immunohistochemical staining of typical proinflammatory cytokines of UC (TNF- $\alpha$ , IL-1 $\beta$ , and IL-6) of transverse sections of mice colon and (B to D) corresponding positive area of proinflammatory proteins. (E to G) The concentration of proinflammatory proteins of lysate of homogenized colonic tissues detected by ELISA assay (A-2) Immunofluorescence staining of phenotypic change of macrophages (Red:CD206; Green:CD80) and (H, I) corresponding positive area of macrophages (\*\* $P < 0.001$ , \* $P < 0.01$ , \* $P < 0.05$ ,  $n \geq 3$ ). (For interpretation of the references to color in this figure legend, the reader is referred to the Web version of this article.)

The microscopic morphology of colon was further evaluated by HE staining and MPO staining. Results were shown in Fig. 6F. There was the severely collapsed crypt, the disrupted epithelium and massive infiltration of inflammatory cells in colon for DSS-induced colitis mice. Meanwhile, the higher level of MPO was also observed in colon for this group. Na-MMT treatment did not obviously reverse this pathogenesis. But the significant decreased MPO activity and the regular colonic morphology

was observed after PDA/MMT treatment, demonstrating its great therapeutic outcome for colitis (Fig. 6H/I).

### 3.6. PDA/MMT alleviated inflammatory response

UC is characterized by the superficial inflammation, which mainly affect mucosa (Fig. S5). IHC staining of inflammatory cytokines were

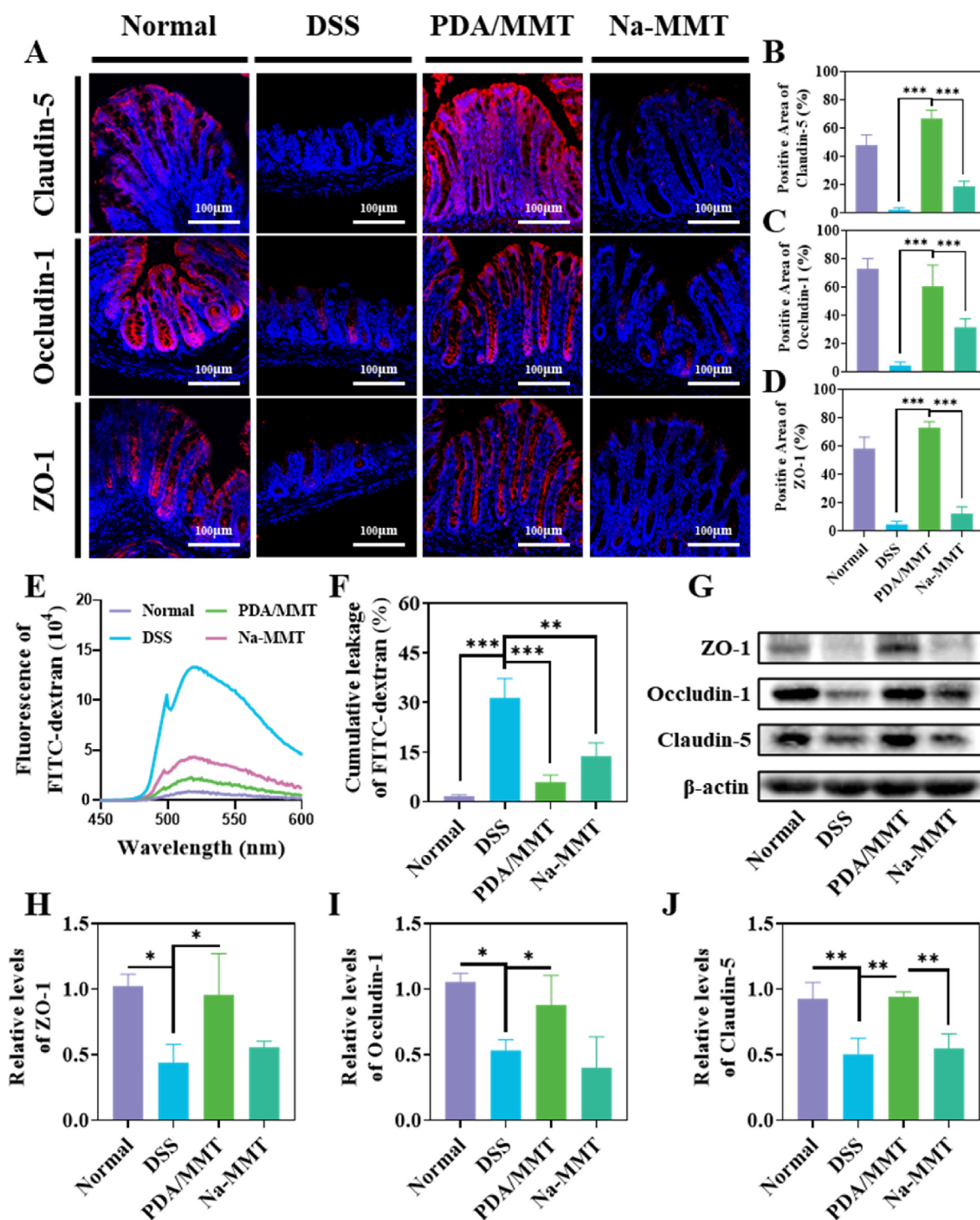


**Fig. 8.** PDA/MMT recovered the intestinal mucosal barrier *in vivo*. (A) Immunofluorescent staining of Occludin-1 (OCLN-1), claudin-5 (CLDN-5), and zonula occludens-1 (ZO-1) and (B-D) corresponding quantitative analysis of the fluorescent area ratio of tight junctions (blue: DAPI, cell nucleus; red: tight junction proteins). (E-F) Blood fluorescent intensity of mice after enema FITC-dextran. (G) Western Blot of tight junctions and (H-J) semi-quantification of protein content. (\*\*\* $P < 0.001$ , \*\* $P < 0.01$ , \* $P < 0.05$ ,  $n \geq 3$ ). (For interpretation of the references to color in this figure legend, the reader is referred to the Web version of this article.)

showed in Fig. 7A–D. The pro-inflammatory cytokines (TNF- $\alpha$ , IL-1 $\beta$ , and IL-6) was mainly accumulated in the goblet cells and epithelium of colon for DSS-induced mouse. The obvious inhibition of these cytokines in colonic mucosa was observed after PDA/MMT treatment. The quantitative analysis of these proinflammatory cytokines in colon was further conducted by ELISA kits. These cytokines in PDA/MMT group were decreased to the comparable level of normal group, while other treatments still present the obviously higher levels of cytokines than healthy mouse (Fig. 7E–G). Massive macrophages are resided in submucosa of colon, which regulate the immune inflammation and tissue wound remodeling. Macrophages presents two phenotypes, that is, inflammation-associated M1-typed macrophages and anti-inflammatory M2-typed macrophages. M1-differentiated macrophages induce an inflammatory response through releasing pro-inflammatory cytokine, while M2-differentiated macrophages secrete anti-inflammatory cytokines to alleviate inflammation [53]. The phenotypic change from the M1 to M2 is a vital factor for influencing the inflammatory outcome of UC [4]. CD80, a maker of M1 macrophage were significantly inhibited after PDA/MMT treatment or Na-MMT treatment (Fig. 7A). While CD206, a marker of M2 macrophage was obviously enhanced by PDA/MMT treatment rather than Na-MMT treatment (Fig. 7H/I). These result implicate that PDA-MMT can promote the polarizing change of macrophage from M1 to M2 phenotype.

### 3.7. PDA/MMT recovered the intestinal mucosal barrier

It is key for UC treatment to restore the epithelial barrier integrity and maintain its physiology function of the insulted colon [54]. Destroyed intestinal barrier allows the luminal antigens, e.g., bacterium-derived

antigens to translocate into the gut wall and thus results in chronic mucosal immune inflammation. The mucosal barrier is mainly composed of the renewable mucus layer and epithelial cells [56]. Tight junction-related proteins (TJs) between the intestinal epithelium are the key regulatory factors of the mucosal barrier [57]. TJs molecules, e.g., OCLN-1, claudin-5 (CLDN-5), and zonula occludens-1 (ZO-1) in colonic mucosa were stained and results were shown in Fig. 8A. DSS treatment down-regulated the expression of TJs in the colonic epithelial layer, which was counteracted by PDA/MMT treatment (Fig. 8B/C/D). Up-regulating TJs expressions after PDA/MMT treatment were further verified by western blot assay. Especially, the level of CLDN-5 or ZO-1 was recovered to the level of healthy mouse. By contrast, there was not obvious improvement of these TJs for Na-MMT treatment. The relative level of CLDN-5 or ZO-1 for Na-MMT group decreased by ~50% in comparison with normal mouse (Fig. 8G–J). This result may due to the fact that Na-MMT acting as a temporary barrier is not effective enough to promote the recovery of mucosal barrier [24]. The mucosal barrier healing for PDA/MMT may be associated with the simultaneously eliminating harmful factors such as excess ROS and pro-inflammatory cytokines.

The epithelial permeability was assessed by infusing FITC-dextran and results were shown in Fig. 8E/F. The high concentration of FITC-dextran in blood was presented for DSS-induced colitis mouse, indicating the severe disruption of the epithelial barrier. The decrease of the blood concentration of FITC-dextran was 56% after PDA/MMT treatment. While the blood concentration of FITC-dextran after PDA/MMT decreased by 81% in comparison to DSS group. These results indicated that PDA/MMT more effectively restore the gut barrier. This may be due to the integrity of the broad spectra of ROS scavenging, the nourishing

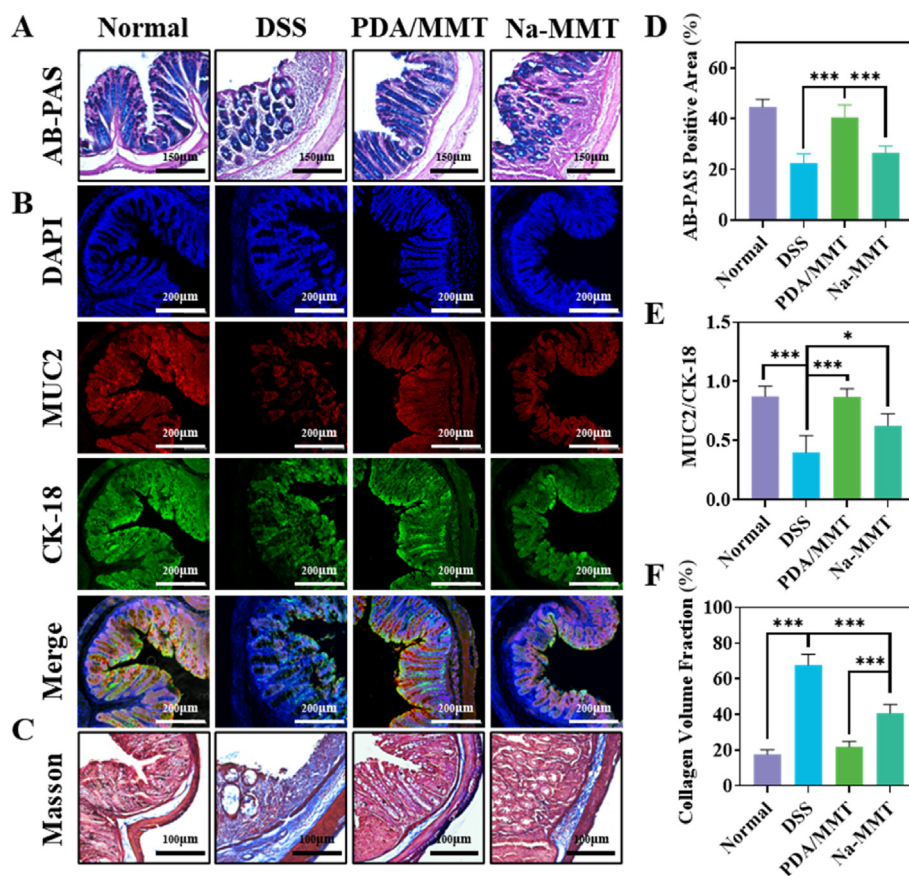


**Fig. 9.** PDA/MMT recovered the mucosal secretion and prevent fibrosis *in vivo*. (A) AB-PAS staining, (B) Immunofluorescent staining of goblet cells biomarker, and (C) Masson trichrome staining of transverse sections of mice colon. Quantitative analysis of the glycosylated mucus and goblet cells based on (D) AB-PAS staining and (E) MUC2<sup>+</sup>CK18<sup>+</sup> staining. (F) Quantitative analysis of the collagen volume based on Masson staining (\*\**P* < 0.001, \*\**P* < 0.01, \**P* < 0.05, *n* ≥ 3).

mucosa and the temporary barrier formation of PDA/MMT at colon lumen [24]. The current therapies for mucosal healing were either inhibiting immune response or combating the particular inflammatory chemicals. Unlike the current therapeutics, PDA/MMT is used as therapeutic platform without risk of systemic infection and the common steroids-relevant side effects [55].

### 3.8. PDA/MMT recovered the mucosal secretion and prevent fibrosis

The goblet cells secrete mucopolysaccharide and the glycosylated mucins protein, forming a mucus barrier on colonic mucosa. Mucus barrier prevents the exposure of invasive pathogens to the epithelium and thereby attenuates the disordered immunity [58]. The glycosylated mucus layer on epithelium was first determined by Alcian Blue Periodic Acid Schiff (AB-PAS) staining. The dysregulated mucin production and vacuolation of secretory structure were observed in DSS-induced colitis. This physiological damage was not improved after Na-MMT treatment. But it was effectively reversed by PDA/MMT treatment (Fig. 9A/D). Apart from restoring mucin, the functional goblet cells (MUC2<sup>+</sup> CK18<sup>+</sup>) were also stained. In line with the result of AB-PAS staining, the functional goblet cells were mainly distributed around epithelium and were dramatically destroyed in the colon section with DSS-induced colitis (Fig. 9B/E). Part of functional goblet cells were recovered by Na-MMT treatment, which may be attributed to the nourishing and mucosal protective effect of Na-MMT [59]. It's been reported that MMT increases the strength of mucus via binding to mucus glycoproteins and thus reduces the loss of water and electrolytes [22,60,61]. But they were effectively restored by PDA/MMT treatment. This may be associated with the broad spectra of ROS scavenging of PDA/MMT.

Intestinal fibrosis is a common complication of UC, being implicated in the remodeling and destruction of gut. It is well established that oxidative damage and inflammation are two keys to initiate fibrosis. Colitis-

relevant fibrosis was also detected by Masson's trichrome staining. As expected, massive collagen was deposited in the mucosa or submucosa of the damaged colon in DSS-induced colitis mouse (Fig. 9C/F). Similarly, Na-MMT treatment failed to prevent collagen deposition in the intestinal submucosa. But PDA/MMT treatment effectively restored intestinal epithelial morphology and suppressed intestinal fibrosis. These results were in accord with the results of previous study showing that persistent inflammation of the colon can lead to tissue tumefaction due to abnormal hyperplasia of collagen fibers. PDA/MMT as a therapeutic platform may provide a rational approach to prevent fibrosis in colitis.

### 3.9. PDA/MMT inhibited oxidative stress of inflamed colon

To elucidate the therapeutic mechanism of PDA/MMT against colitis, the ROS level in colon was measured by DCFH-DA staining of frozen colon slices. Strong green fluorescence was present in the colon of DSS-induced colitis mice (Fig. 10A/C), indicating the disrupted redox homeostasis. Besides, oxidative stress in colon was also demonstrated by high levels of iNOS. After PDA/MMT treatment, there was an obvious decrease in the colonic ROS and iNOS (Fig. 10B/D). Alternatively, the intracellular redox-related enzymes and products were also detected and the result was shown in Fig. 10E. The relative concentration of superoxide dismutase (SOD) was as low as 20 U/mg protein in UC. But it was recovered to the comparable levels of healthy mice after PDA/MMT treatment. Myeloperoxidase (MPO) participates in immune and inflammatory responses by generating toxic radicals, and catalyzes excessive ROS generation. Excessive ROS, exceeding the defense response of local antioxidants, finally leads to oxidative stress and oxidative tissue damage. PDA/MMT significantly relieved the colonic MPO level, which decreased by 150% in comparison with that of DSS-induced colitis mice (Fig. 10F). Malondialdehyde (MDA) is the cytotoxic product of the peroxidized lipid. The colonic MDA level in DSS-induced colitis mice nearly

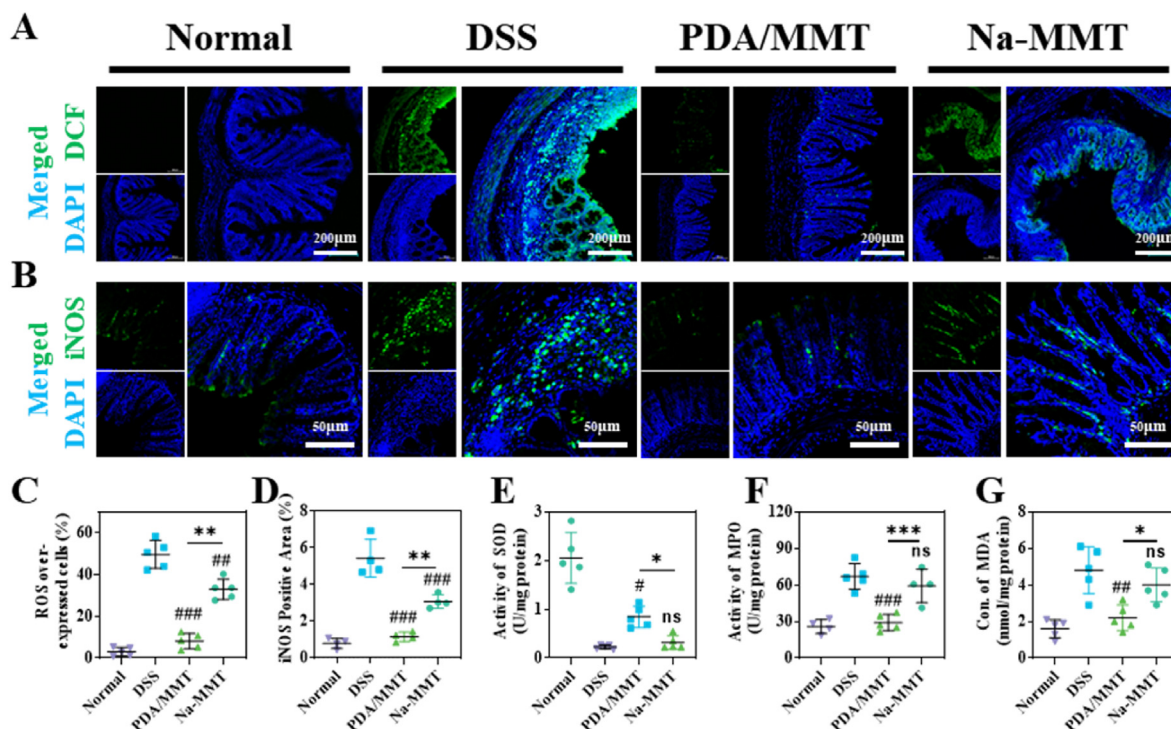


**Fig. 10.** PDA/MMT inhibited oxidative stress *in vivo*. (A) DCF fluorescent staining of frozen mice colon. (blue: DAPI, cell nucleus; green: DCF, intracellular ROS) and (B) immunofluorescence staining of iNOS and Inos and (C to G) corresponding quantitative analysis of the fluorescent area ratio of intracellular ROS and Inos, respectively. Relative *in vivo* expression of (E) superoxide dismutase (SOD), (F) myeloperoxidase (MPO), and (G) malondialdehyde (MDA) (\*\* $P < 0.001$ , \*\* $P < 0.01$ , \* $P < 0.05$ ,  $n \geq 3$ ; and ### $P < 0.001$ , ## $P < 0.01$ , # $P < 0.05$ ,  $n \geq 3$ , vs DSS). (For interpretation of the references to color in this figure legend, the reader is referred to the Web version of this article.)

doubled that of normal mice. After PDA/MMT treatment, the colonic MDA level significantly dropped (Fig. 10G). In general, the living organisms consistently maintain the balance between the generation and the elimination of ROS under antioxidant-protective systems. However, the redox homeostasis balance was broken for the pathogenesis of UC. PDA/MMT was effective to restore the balance and inhibit the oxidative stress of inflamed colon.

#### 4. Conclusions

The conventional treatment of UC suffers from the limited efficacy and systemic side effects. Aberrant oxidative stress was reported to play a vital role in the occurrence and development of UC. Recently developing ROS-scavenging materials have provided several novel anti-oxidative strategies to ameliorate colonic inflammation. Hafnium disulfide atomic crystals and titanium carbide nanosheets were fabricated to target the inflamed colon and eliminate reactive oxygen species [62,63]. Those emerging studies place too much emphasis on the robust antioxidant capacity and ignore the potential threat of long-term toxicity to UC treatment, because of the extremely fragile intestinal homeostasis of UC patients. Oxidative stress and gut mucosal injury constitute two key pathogenic hallmarks for patients with ulcerative colitis (UC). Montmorillonite (MMT), an inorganic mineral layered aluminosilicate, has a mucosal nutrient effect and restores the integrity of intestinal barriers. However, it is not effective for orally administering MMT to combat the reactive oxygen species (ROS) and alleviate the acute inflammatory relapse. Herein, polydopamine-cladded montmorillonite micro-sheets (PDA/MMT) as a therapeutic platform was novelty fabricated by the oxidative polymerization of dopamine monomer (DA) on surface of Na-MMT in alkaline condition. PDA/MMT presents the broad spectra of scavenging various ROS sources including  $\bullet\text{OH}$ ,  $\bullet\text{O}_2^-$ , and  $\text{H}_2\text{O}_2$ . PDA/MMT could also largely scavenge the intracellular ROS of Rosup/ $\text{H}_2\text{O}_2$  treated Caco-2 cells and thus improve the cell viability under oxidative stress. Most of orally administrated PDA/MMT was transited to the gut and form a protective film on diseased colon. PDA/MMT as a therapeutic platform present the more obvious alleviating effect on the colonic inflammation and repairing the gut mucosa of colitis mouse than naïve MMT. After PDA/MMT treatment, the level of MDA and iNOS in colon decrease by 2.2-fold and 4.9-fold, respectively, while the level of SOD increase by 3.8-fold. PDA/MMT treatment relieve the oxidative stress of the insulted colon and promoted the polarizing of macrophage from an inflammatory (M1) to anti-inflammatory (M2) phenotype. Collectively, PDA/MMT micro-sheets as a therapeutic platform may provide a promising therapeutic strategy for UC treatment.

#### Credit author statement

We would like to submit the enclosed manuscript entitled “*Polydopamine-cladded montmorillonite micro-sheets as therapeutic platform repair the gut mucosal barrier of murine colitis through inhibiting oxidative stress*” by Gaolong Lin, Fengnan Yu, Dingwei Li, Yi Chen, Mengjiao Zhang, Kaili Lu, Neili Wang, Sunkuan Hu, Yingcheng Zhao, Helin Xu, which we wish to be considered for publication in “Materials Today Bio”. No conflict of interest exists in the submission of this manuscript, and manuscript is approved by all authors for publication. I would like to declare on behalf of my co-authors that the work described was original research that has not been published previously, and not under consideration for publication elsewhere, in whole or in part.

#### Authors contribution

Gaolong Lin: Original draft preparation, Fengnan Yu and Dingwei Li: Methodology, Visualization, Investigation, Mengjiao Zhang and Kaili Lu: Visualization, Investigation, Neili Wang: Software, Sunkuan Hu: Validation, Yingcheng Zhao: Supervision, Helin Xu: Conceptualization and Writing- Reviewing and Editing.

#### Declaration of competing interest

The authors declare that they have no known competing financial interests or personal relationships that could have appeared to influence the work reported in this paper.

#### Data availability

Data will be made available on request.

#### Acknowledgments

This research was supported by Wenzhou Scientific and Technological innovation project (Grant No. ZY2022025), Ningbo Science and Technology Bureau (Grant No. 2022J047), Zhejiang Provincial Foundation for Health Department (Grant No. 2021KY198), Wenzhou Science and Technology Bureau (Grant No. Y20210211), Excellent youth talents of Wenzhou Medical University (H-L Xu) and Scientific research project of Wenzhou Medical University (Grant No. XY2022005).

#### Appendix A. Supplementary data

Supplementary data to this article can be found online at <https://doi.org/10.1016/j.mtbio.2023.100654>.

#### References

- [1] M. Camilleri, L. Buéno, V. Andresen, et al., Pharmacologic, pharmacokinetic, and pharmacogenomic aspects of functional gastrointestinal disorders [J], *Gastroenterology* 150 (6) (2016) 1319–1331.e20.
- [2] H.S.P. De Souza, C. Focchi, D. Iliopoulos, The IBD interactome: an integrated view of aetiology, pathogenesis and Therapy [J], *Nat. Rev. Gastroenterol. Hepatol.* 14 (12) (2017) 739–749.
- [3] T. Kobayashi, B. Siegmund, C. Le Berre, et al., Ulcerative colitis [J], *Nat. Rev. Dis. Prim.* 6 (1) (2020) 74.
- [4] J.T. Chang, Pathophysiology of inflammatory bowel diseases [J], *N. Engl. J. Med.* 383 (27) (2020) 2652–2664.
- [5] S. Alatab, S.G. Sepanlou, K. Ikuta, et al., The global, regional, and national burden of inflammatory bowel disease in 195 countries and territories, 1990–2017: a systematic analysis for the Global Burden of Disease Study 2017 [J], *Lancet Gastroenterol. Hepatol.* 5 (1) (2020) 17–30.
- [6] V. Stanghellini, F.K.L. Chan, W.L. Hasler, et al., Gastrointestinal disorders [J], *Gastroenterology* 150 (6) (2016) 1380–1392.
- [7] D.C. Baumgart, C. Le Berre, Newer biologic and small-molecule therapies for inflammatory bowel disease [J], *N. Engl. J. Med.* 385 (14) (2021) 1302–1315.
- [8] A.-C. Luissint, C.A. Parkos, A. Nusrat, Inflammation and the intestinal barrier: leukocyte–epithelial cell interactions, cell junction remodeling, and mucosal repair [J], *Gastroenterology* 151 (4) (2016) 616–632.
- [9] A. Bhattacharyya, R. Chattopadhyay, S. Mitra, et al., Oxidative stress: an essential factor in the pathogenesis of gastrointestinal mucosal diseases [J], *Physiol. Rev.* 94 (2) (2014) 329–354.
- [10] B. Yang, Y. Chen, J. Shi, Reactive oxygen species (ROS)-Based nanomedicine [J], *Chem. Rev.* 119 (8) (2019) 4881–4985.
- [11] S. Pérez, R. Taléns-Visconti, S. Rius-Pérez, et al., Redox signaling in the gastrointestinal Tract [J], *Free Radic. Biol. Med.* 104 (3) (2017) 75–103.
- [12] A. Bhattacharyya, R. Chattopadhyay, S. Mitra, et al., Oxidative stress: an essential factor in the pathogenesis of gastrointestinal mucosal diseases [J], *Physiol. Rev.* 94 (2) (2014) 329–354.
- [13] F.A. Moura, K.Q. De Andrade, J.C.F. Dos Santos, et al., Antioxidant therapy for treatment of inflammatory bowel disease: does it Work? [J], *Redox Biol.* 6 (3) (2015) 617–639.
- [14] Z. Zeng, X. He, C. Li, et al., Oral delivery of antioxidant enzymes for effective treatment of inflammatory Disease [J], *Biomaterials* 271 (8) (2021), 120753.
- [15] W. Han, A. Mercenier, A. Ait-Belgnaoui, et al., Improvement of an experimental colitis in rats by lactic acid bacteria producing superoxide Dismutase [J], *Inflamm. Bowel Dis.* 12 (11) (2006) 1044–1052.
- [16] Y. Liu, Y. Cheng, H. Zhang, et al., Integrated cascade nanozyme catalyzes in vivo ROS scavenging for Anti-inflammatory Therapy [J], *Sci. Adv.* 6 (29) (2020), eabb2695.
- [17] H. Guo, H. Guo, Y. Xie, et al., Mo3Se4 nanoparticle with ROS scavenging and Multi-enzyme activity for the treatment of DSS-induced colitis in Mice [J], *Redox Biol.* 56 (8) (2022), 102441.
- [18] J. Yang, J. Zhou, Y. Zhao, et al., Hollow CeO2 with ROS-scavenging activity to alleviate colitis in mice [J], *Int. J. Nanomed.* 16 (4) (2021) 6889–6904.
- [19] L. Hou, F. Gong, B. Liu, et al., Orally administered titanium carbide nanosheets as Anti-inflammatory therapy for Colitis [J], *Theranostics* 12 (8) (2022) 3834–3846.
- [20] C. Dupont, B. Vernisse, Anti-diarrheal effects of diosmetecite in the treatment of acute diarrhea in children [J], *Pediatr. Drugs* 11 (2) (2009) 89–99.

- [21] L.Z. Zhao, C.H. Zhou, J. Wang, et al., Recent advances in clay Mineral-containing nanocomposite Hydrogels [J], *Soft Matter* 11 (48) (2015) 9229–9246.
- [22] M.T. Droy-Lefaix, F. Tateo, *Clays and Clay Minerals as Drugs* [M], Elsevier, 2006, pp. 743–752.
- [23] V. Iannucelli, E. Maretta, M. Montorsi, et al., Gastroretentive montmorillonite-tetracycline nanoclay for the treatment of *Helicobacter pylori* infection [J], *Int. J. Pharm.* 493 (1–2) (2015) 295–304.
- [24] H. Zhao, H. Ye, J. Zhou, et al., Montmorillonite-enveloped zeolitic imidazolate framework as a nourishing oral nano-platform for gastrointestinal drug delivery [J], *ACS Appl. Mater. Interfaces* 12 (44) (2020) 49431–49441.
- [25] V. Ball, D. Del Frari, M. Michel, et al., Deposition mechanism and properties of thin polydopamine films for high added value applications in surface science at the Nanoscale [J], *BioNanoSci.* 2 (1) (2011) 16–34.
- [26] F. Bernsmann, V. Ball, F. Addiego, et al., Dopamine–Melanin film deposition depends on the used oxidant and buffer solution [J], *Langmuir* 27 (6) (2011) 2819–2825.
- [27] S. El Yakhli, V. Ball, Polydopamine as a stable and functional Nanomaterial [J], *Colloids Surf. B Biointerfaces* 186 (2) (2020), 110719.
- [28] V. Ball, D.D. Frari, V. Toniazio, et al., Kinetics of polydopamine film deposition as a function of pH and dopamine concentration: insights in the polydopamine deposition Mechanism [J], *J. Colloid Interface Sci.* 386 (1) (2012) 366–372.
- [29] J. Hu, L. Yang, P. Yang, et al., Polydopamine free radical Scavengers [J], *Biomater. Sci.* 8 (18) (2020) 4940–4950.
- [30] H. Liu, X. Qu, H. Tan, et al., Role of polydopamine's redox-activity on its pro-oxidant, radical-scavenging, and antimicrobial Activities [J], *Acta Biomater.* 88 (6) (2019) 181–196.
- [31] X. Bao, J. Zhao, J. Sun, et al., Polydopamine nanoparticles as efficient scavengers for reactive oxygen species in periodontal disease [J], *ACS Nano* 12 (9) (2018) 8882–8892.
- [32] L. Wang, Z. Wang, Y. Pan, et al., Polycatechol-derived mesoporous polydopamine nanoparticles for combined ROS scavenging and gene interference therapy in inflammatory bowel disease [J], *ACS Appl. Mater. Interfaces* 14 (17) (2022) 19975–19987.
- [33] W. Cheng, X. Zeng, H. Chen, et al., Versatile polydopamine platforms: synthesis and promising applications for surface modification and advanced nanomedicine [J], *ACS Nano* 13 (8) (2019) 8537–8565.
- [34] W. Xu, J. Peng, D. Ni, et al., Preparation, characterization and application of levan/montmorillonite biocomposite and levan/BSA Nanoparticle [J], *Carbohydrate Polym.* 234 (8) (2020), 115921.
- [35] V.K.K. Paravastu, S.R. Yarraguntla, A. Suvvari, Role of nanocomposites in drug Delivery [J], *GSC Biol. Pharmaceut. Sci.* 8 (3) (2019) 94–103.
- [36] H. Lee, S.M. Dellatore, W.M. Miller, et al., Mussel-Inspired surface chemistry for multifunctional coatings [J], *Science* 318 (5849) (2007) 426–430.
- [37] N. Zhao, F. Yang, C. Zhao, et al., Construction of pH-dependent nanozymes with oxygen vacancies as the high-efficient reactive oxygen species scavenger for oral-administrated anti-inflammatory therapy [J], *Advan. Healthcare Mater.* 10 (23) (2021), 2101618.
- [38] F.S. Samman, S.M. Elaidy, S.S. Essawy, et al., New insights on the modulatory roles of metformin or Alpha-lipoic acid versus their combination in dextran sulfate sodium-induced chronic colitis in Rats [J], *Pharmacol. Rep.* 70 (3) (2018) 488–496.
- [39] X. Zhang, X. Zhao, S. Tie, et al., A smart Cauliflower-like carrier for astaxanthin delivery to relieve colon Inflammation [J], *J. Contr. Release* 342 (2022) 372–387.
- [40] S. Matsuo, W.-L. Yang, M. Aziz, et al., Fatty acid synthase inhibitor C75 ameliorates experimental colitis [J], *Mol. Med.* 20 (1) (2013) 1–9.
- [41] K.J. Maloy, F. Powrie, Intestinal homeostasis and its breakdown in inflammatory bowel Disease [J], *Nature* 474 (7351) (2011) 298–306.
- [42] C.-C. Wang, L.-C. Juang, T.-C. Hsu, et al., Adsorption of basic dyes onto Montmorillonite [J], *J. Colloid Interface Sci.* 273 (1) (2004) 80–86.
- [43] S. Hong, Y.S. Na, S. Choi, et al., Non-covalent self-assembly and covalent polymerization Co-contribute to polydopamine formation [J], *Adv. Funct. Mater.* 22 (22) (2012) 4711–4717.
- [44] Y.E. Kim, J. Kim, ROS-scavenging therapeutic hydrogels for modulation of the inflammatory response [J], *ACS Appl. Mater. Interfaces* 14 (20) (2021) 23002–23021.
- [45] L. Wang, Z. Wang, Y. Pan, et al., Polycatechol-derived mesoporous polydopamine nanoparticles for combined ROS scavenging and gene interference therapy in inflammatory bowel disease [J], *ACS Appl. Mater. Interfaces* 14 (17) (2022) 19975–19987.
- [46] W. Fan, S. Zhang, Y. Wu, et al., Genistein-derived ROS-responsive nanoparticles relieve colitis by regulating mucosal homeostasis [J], *ACS Appl. Mater. Interfaces* 13 (34) (2021) 40249–40266.
- [47] R. Wang, H. Li, G. Ge, et al., Montmorillonite-based two-dimensional nanocomposites: preparation and applications [J], *Molecules* 26 (9) (2021) 2521.
- [48] W. Xiong, Y. Wu, K.-Y. Sun, et al., Ultrathin niobium carbide alleviates colitis through absorbing ROS [J], *Mater. Des.* 213 (2022), 110351.
- [49] C. Zhang, X. Wang, J. Du, et al., Reactive oxygen species-regulating strategies based on nanomaterials for disease treatment [J], *Adv. Sci.* (2020), 2002797.
- [50] S. Bertoni, Z. Liu, A. Correia, et al., PH and reactive oxygen species-sequential responsive nano-in-micro composite for targeted therapy of inflammatory bowel disease [J], *Adv. Funct. Mater.* 28 (50) (2018), 1806175.
- [51] H. Simon, A. Haj-Yehia, F. Levi-Schaffer, Role of reactive oxygen species (ROS) in apoptosis Induction [J], *Apoptosis* (2000).
- [52] V.O. Kaminsky, B. Zhivotovsky, Free radicals in cross talk between autophagy and apoptosis [J], *Antioxidants Redox Signal.* 21 (1) (2014) 86–102.
- [53] S. Zhao, Y. Li, Q. Liu, et al., An orally administered CeO<sub>2</sub>@MMT nanozyme targets inflammation for inflammatory bowel disease therapy [J], *Adv. Funct. Mater.* 30 (45) (2020), 2004692.
- [54] P. Zhao, X. Xia, X. Xu, et al., Nanoparticle-assembled bioadhesive coacervate coating with prolonged gastrointestinal retention for inflammatory bowel disease Therapy [J], *Nat. Commun.* 12 (1) (2021).
- [55] Y. Tian, J. Xu, Y. Li, et al., MicroRNA-31 reduces inflammatory signaling and promotes regeneration in colon epithelium, and delivery of mimics in microspheres reduces colitis in mice [J], *Gastroenterology* 156 (8) (2019) 2281–2296.e6.
- [56] E.J. Villablanca, K. Selin, C.R.H. Hedin, Mechanisms of mucosal healing: treating inflammatory bowel disease without Immunosuppression? [J], *Nat. Rev. Gastroenterol. Hepatol.* 19 (8) (2022) 493–507.
- [57] Q. Mao, H. Pan, Y. Zhang, et al., GelNB molecular coating as a biophysical barrier to isolate intestinal irritating metabolites and regulate intestinal microbial homeostasis in the treatment of inflammatory bowel Disease [J], *Bioact. Mater.* 19 (2023) 251–267.
- [58] Y. Zhao, P. Xue, G. Lin, et al., A KPv-binding double-network hydrogel restores gut mucosal barrier in an inflamed Colon [J], *Acta Biomater.* 143 (2022) 233–252.
- [59] T. Pelaseyed, J.H. Bergström, J.K. Gustafsson, et al., The mucus and mucins of the goblet cells and enterocytes provide the first defense line of the gastrointestinal tract and interact with the immune System [J], *Immunol. Rev.* 260 (1) (2014) 8–20.
- [60] Q. Wang, J. Shen, E. Mo, et al., A versatile ultrafine and Super-absorptive H<sup>+</sup>-modified montmorillonite: application for metabolic syndrome intervention and gastric mucosal Protection [J], *Biomater. Sci.* 8 (12) (2020) 3370–3380.
- [61] C. Feng, J. Li, M. Kong, et al., Surface charge effect on mucoadhesion of chitosan based nanogels for local Anti-colorectal cancer drug Delivery [J], *Colloids Surf. B Biointerfaces* 128 (2015) 439–447.
- [62] R. Surya, M.D. Mullasery, N.B. Fernandez, et al., Synthesis and characterization of a pH responsive and mucoadhesive drug delivery system for the controlled release application of Anti-cancerous Drug [J], *Arab. J. Chem.* 13 (5) (2020) 5262–5276.
- [63] L. Wang, J. Xu, P. Xue, et al., Thermo-sensitive hydrogel with mussel-inspired adhesion enhanced the non-fibrotic repair effect of EGF on colonic mucosa barrier of TNBS-induced ulcerative colitis rats through macrophage Polarizing [J], *Chem. Eng. J.* 416 (2021), 129221.